



## **Incorporating diffuse radiation into a light use efficiency and evapotranspiration model: An 11-year study in a high latitude deciduous forest**

**Wang, Sheng; Ibrom, Andreas; Bauer-Gottwein, Peter; Garcia, Monica**

*Published in:*  
Agricultural and Forest Meteorology

*Link to article, DOI:*  
[10.1016/j.agrformet.2017.10.023](https://doi.org/10.1016/j.agrformet.2017.10.023)

*Publication date:*  
2018

*Document Version*  
Peer reviewed version

[Link back to DTU Orbit](#)

*Citation (APA):*  
Wang, S., Ibrom, A., Bauer-Gottwein, P., & Garcia, M. (2018). Incorporating diffuse radiation into a light use efficiency and evapotranspiration model: An 11-year study in a high latitude deciduous forest. *Agricultural and Forest Meteorology*, 248, 479-493. <https://doi.org/10.1016/j.agrformet.2017.10.023>

---

### **General rights**

Copyright and moral rights for the publications made accessible in the public portal are retained by the authors and/or other copyright owners and it is a condition of accessing publications that users recognise and abide by the legal requirements associated with these rights.

- Users may download and print one copy of any publication from the public portal for the purpose of private study or research.
- You may not further distribute the material or use it for any profit-making activity or commercial gain
- You may freely distribute the URL identifying the publication in the public portal

If you believe that this document breaches copyright please contact us providing details, and we will remove access to the work immediately and investigate your claim.

1 Incorporating diffuse radiation into a light use efficiency and evapotranspiration model:  
2 an 11-year study in a high latitude deciduous forest

3 Sheng Wang<sup>a\*</sup>, Andreas Ibrom<sup>a</sup>, Peter Bauer-Gottwein<sup>a</sup>, Monica Garcia<sup>a,b</sup>

4 a. Department of Environmental Engineering, Technical University of Denmark, 2800 Kgs. Lyngby, Denmark; b.  
5 International Research Institute for Climate and Society, The Earth Institute, Columbia University, Palisades,  
6 NY (USA)

7 \*corresponding author: [swan@env.dtu.dk](mailto:swan@env.dtu.dk)

8 **Abstract:**

9 The fraction of diffuse photosynthetic active radiation (PAR) reaching the land surface is one of the biophysical  
10 factors regulating carbon and water exchange between ecosystems and the atmosphere. This is especially  
11 relevant for high latitude ecosystems, where cloudy days are prevalent. Without considering impacts of diffuse  
12 PAR, traditional ‘top-down’ models of ecosystem gross primary productivity (GPP) and evapotranspiration (ET),  
13 which use satellite remote sensing observations, tend to be biased towards clear sky conditions. Thus, this study  
14 incorporated a cloudiness index (CI), an index for the fraction of diffuse PAR, into a joint ‘top-down’ model that  
15 uses the same set of biophysical constraints to simulate GPP and ET for a high latitude temperate deciduous  
16 forest. To quantify the diffuse PAR effects, CI along with other environmental variables derived from an eleven-  
17 year eddy covariance data set were used to statistically explore the independent and joint effects of diffuse PAR  
18 on GPP, ET, incident light use efficiency (LUE), evaporative fraction (EF) and ecosystem water use efficiency  
19 (WUE). The independent and joint effects of CI were compared from global sensitivity analysis of the ‘top-down’  
20 models. Results indicate that for independent effects, CI increased GPP, LUE, ET, EF and WUE, but analysis of  
21 joint effects shows that as CI mainly interacted with the radiation intercepted in the canopy (PAR, net radiation  
22 and leaf area index) to influence GPP, ET and WUE. Moreover,  $T_a$  and vapor pressure deficit played a major  
23 role for the joint influence of CI on LUE and EF. We quantified that CI contributes 11.88%, 3.04% and 7.78% to  
24 the total variation of GPP, ET and transpiration in the growing season from May to October, respectively. As the  
25 influence of CI on GPP is larger than that on ET, this leads to an increase in WUE. Joint GPP and ET model  
26 results showed that when including CI, the root mean square errors (RMSE) of daily GPP decreased from 1.64 to  
27 1.45  $\text{g}\cdot\text{C}\cdot\text{m}^{-2}\cdot\text{d}^{-1}$  (11.68% reduction) and ET from 15.79 to 14.50  $\text{W}\cdot\text{m}^{-2}$  (8.16% reduction). Due to the interaction  
28 of diffuse PAR with plant canopies, the largest model improvements using CI for GPP and ET occurred during  
29 the growing season and for the transpiration component, as suggested by comparisons to sap flow measurements.  
30 Furthermore, our study suggests a potential biophysical mechanism, not considered in other studies: due to the  
31 increased longwave emission from clouds, surface temperature gets higher and closer to optimum, boosting GPP  
32 and transpiration in the temperature-limited high latitude ecosystem.

33 **Key words:** diffuse PAR fraction; eddy covariance; gross primary production; evapotranspiration; ‘top-down’  
34 models; light use efficiency model; Priestley–Taylor Jet Propulsion Laboratory evapotranspiration model

35

36 Table of abbreviations and symbols:

37 *Latin alphabet*

- 38 • CI: cloudiness index (dimensionless)
- 39 • EF: evaporative fraction (dimensionless)
- 40 • ET: evapotranspiration ( $\text{mm}\cdot\text{d}^{-1}$ )
- 41 •  $f_{\text{APAR}}$ : fraction of absorbed PAR (dimensionless)
- 42 •  $f_{\text{ci}}$ : cloudiness index constraint (dimensionless)
- 43 •  $f_{\text{diff}}$ : fraction of diffuse PAR (dimensionless)
- 44 •  $f_g$ : the green canopy fraction indicating the proportion of active canopy (dimensionless)
- 45 •  $f_M$ : the plant moisture constraint (dimensionless)
- 46 •  $f_{\text{IPAR}}$ : fraction of intercepted PAR (dimensionless)
- 47 •  $f_{\text{Ta}}$ : the air temperature constraint reflecting the temperature limitation of photosynthesis (dimensionless)
- 48 •  $f_{\text{SWC}}$ : the soil moisture constraint on photosynthesis (dimensionless)
- 49 •  $f_{\text{VPD}}$ : the VPD constraint reflecting the stomatal response to the atmospheric water saturation deficit
- 50 (dimensionless)
- 51 • G: Ground heat flux ( $\text{W}\cdot\text{m}^{-2}$ )
- 52 • GPP: gross primary productivity ( $\text{g}\cdot\text{C}\cdot\text{m}^{-2}\cdot\text{d}^{-1}$ )
- 53 •  $k_{\text{PAR}}$ : the extinction coefficients for PAR (0.5, dimensionless)
- 54 •  $k_{\text{Rn}}$ : the extinction coefficients for Rn (0.6, dimensionless)
- 55 • LAI: leaf area index ( $\text{m}^2\cdot\text{m}^{-2}$ )
- 56 • LUE: incident light use efficiency ( $\text{g}\cdot\text{C}\cdot\text{MJ}^{-1}$ )
- 57 •  $\text{LW}_{\text{in}}$ : incoming longwave radiation ( $\text{W}\cdot\text{m}^{-2}$ )
- 58 •  $\text{LW}_{\text{out}}$ : outgoing longwave radiation ( $\text{W}\cdot\text{m}^{-2}$ )
- 59 • NDVI: normalized difference vegetation index (dimensionless)
- 60 • PAR: photosynthetically active radiation ( $\text{MJ}\cdot\text{m}^{-2}\cdot\text{d}^{-1}$ )
- 61 •  $\text{PAR}_{\text{c}}$ : PAR intercepted by the canopy ( $\text{MJ}\cdot\text{m}^{-2}\cdot\text{d}^{-1}$ )
- 62 • RH: the relative humidity (dimensionless)
- 63 • Rn: Net radiation ( $\text{W}\cdot\text{m}^{-2}$ )
- 64 •  $\text{Rn}_{\text{c}}$ : Net radiation intercepted by the canopy ( $\text{W}\cdot\text{m}^{-2}$ )
- 65 •  $\text{Rn}_{\text{s}}$ : Net radiation reaching to the soil ( $\text{W}\cdot\text{m}^{-2}$ )
- 66 • SWC: soil water content ( $\text{m}^3\cdot\text{m}^{-3}$ )
- 67 •  $\text{SW}_{\text{in}}$ : incoming shortwave radiation ( $\text{W}\cdot\text{m}^{-2}$ )

- 68 • SZA: sun zenith angle (rad)
- 69 • Ta: air temperature (°C)
- 70 • Ts: surface temperature (°C)
- 71 • To: optimal air temperature for vegetation growth (°C)
- 72 • VPD: vapor pressure deficit (hPa)
- 73 • WUE: ecosystem water use efficiency ( $\text{g}\cdot\text{C}\cdot\text{kg}^{-1}$ )

74

75 *Greek alphabet*

- 76 •  $\alpha$ : PT coefficient, an empirical ratio of potential evapotranspiration to equilibrium potential
- 77 evapotranspiration (dimensionless)
- 78 •  $\gamma$ : the psychrometric constant ( $0.066 \text{ kPa}\cdot\text{°C}^{-1}$ )
- 79 •  $\Delta$ : the slope of saturation-to-vapor pressure curve ( $\text{kPa}\cdot\text{°C}^{-1}$ )
- 80 •  $\varepsilon$ : surface emissivity (dimensionless)
- 81 •  $\varepsilon_{\text{max}}$ : maximum LUE ( $\text{g}\cdot\text{C}\cdot\text{m}^{-2}\cdot\text{MJ}^{-1}$ )
- 82 •  $\lambda$ : latent heat of vaporization ( $\text{kJ}\cdot\text{kg}^{-1}$ )
- 83 •  $\lambda\text{ET}$ : latent heat flux of evapotranspiration ( $\text{W}\cdot\text{m}^{-2}$ )
- 84 •  $\lambda\text{Ec}$ : latent heat flux from transpiration ( $\text{W}\cdot\text{m}^{-2}$ )
- 85 •  $\lambda\text{Ei}$ : latent heat flux from evaporation of intercepted water ( $\text{W}\cdot\text{m}^{-2}$ )
- 86 •  $\lambda\text{Es}$ : latent heat flux from evaporation of soil water ( $\text{W}\cdot\text{m}^{-2}$ )
- 87 •  $\sigma$ : the Stefan-Boltzmann constant ( $5.670367\times 10^{-8} \text{ kg}\cdot\text{s}^{-3}\cdot\text{K}^{-4}$ )

88

89

90 1. Introduction

91 Quantifying land surface water and carbon fluxes is of critical importance for ecosystem and water resources  
 92 management. The temporal dynamics of land surface carbon and water fluxes are controlled by the interplay of  
 93 various biophysical factors, e.g. climate forcing (solar radiation, water vapor and temperature), atmospheric  
 94 conditions ( $\text{CO}_2$  concentration and nitrogen deposition) and biotic factors (leaf area index and plant functional  
 95 types) (Ciais et al., 2005; Dunn et al., 2007; Wu et al., 2016). Among these biophysical factors, the fraction of  
 96 diffuse photosynthetically active radiation (PAR),  $f_{\text{diff}}$  (the ratio between diffuse and total PAR), has been  
 97 highlighted to have strong implications for the global carbon cycle (Gu et al., 2003; Mercado et al., 2009). It  
 98 could increase the efficiency of photosynthesis, which has been referred to the diffuse fertilization effect  
 99 (Roderick et al., 2001; Kanniah et al., 2012). Further, predictions showed that, at the global scale, aerosols in the  
 100 atmosphere would increase by 36% in 2100 (Heald et al., 2008). Aerosols influence cloud formation and  
 101 increase  $f_{\text{diff}}$  in the atmosphere (Schiermeier, 2006). This is especially important for high latitude ecosystems,  
 102 which are already exposed to a higher  $f_{\text{diff}}$  due to low solar height and high frequency of overcast and cloudy  
 103 conditions.

104 With more uniform vertical distribution of incoming photosynthetic active radiation (PAR) under cloudy  
105 conditions, both observations and modeling studies have confirmed more active carbon assimilation rates (Gu et  
106 al., 2002; Lloyd et al., 2002; Steiner and Chameides, 2005; Ibrom et al. 2006, Urban et al., 2012). However, the  
107 gross primary productivity (GPP) enhancement depends on local environmental conditions and ecosystem types.  
108 Healy et al. (1998) reported that increasing  $f_{\text{diff}}$  can increase the incident light use efficiency (LUE, defined as the  
109 ratio between GPP and incoming PAR). This increases crop yield by as much as 50% for maize, soybean and  
110 peanuts. According to observations from 10 temperate forest flux sites in USA, Cheng et al. (2015) found that  
111  $f_{\text{diff}}$  explained up to 41% and 17% of seasonal variations in GPP in croplands and forests, respectively. In a  
112 modeling study, Ibrom et al. (2006) found the uniform PAR distribution in the maritime Scottish climate with a  
113 ca. 20% higher  $f_{\text{diff}}$  lead to a 13-14% higher LUE compared to the continental climate in Germany in spruce  
114 canopies. To identify the impacts of  $f_{\text{diff}}$ , the covariance of  $f_{\text{diff}}$  and other environmental factors (Kanniah et al.,  
115 2012) should also be taken into account. For instance, Williams et al. (2016) found that without considering the  
116 covariance between  $f_{\text{diff}}$  and phenology, the GPP enhancement from  $f_{\text{diff}}$  is 260%, while by separating  $f_{\text{diff}}$  and  
117 phenology, the GPP enhancement induced by  $f_{\text{diff}}$  dropped to 22%. Apart from modeling studies at the global  
118 scale (Mercado et al., 2009), few studies have focused on ecosystems in high latitude regions, which are  
119 radiation and temperature limited (van Dijk et al., 2005; Lagergren et al., 2008). In these ecosystems, the  
120 influence of  $f_{\text{diff}}$  and its covariance with other environmental variables should be thoroughly quantified, because  
121 the potential mechanisms influencing GPP and ET might be different from those of water-limited ecosystems.

122 Because photosynthesis and transpiration are closely linked via stomatal behaviors,  $f_{\text{diff}}$  is expected to also have  
123 moderate impacts on land evapotranspiration (ET) and may eventually influence the global hydrological cycle  
124 and the climate system (Knobl and Baldocchi, 2008; Davin and Seneviratne, 2012; Pedruzo-Bagazgoitia et al.,  
125 2017). For instance, the modeling results from the Community Land Model showed that higher  $f_{\text{diff}}$  during 1960–  
126 1990 increased the latent heat flux of evapotranspiration ( $\lambda\text{ET}$ ) in the tropics by  $2.5 \text{ Wm}^{-2}$  (3% of mean) and  
127 reduced global river runoff (Oliveira et al., 2011). By employing the COSMO-CLM2 regional climate model,  
128 Davin and Seneviratne (2012) identified  $f_{\text{diff}}$  could alter the seasonal evaporative fraction (EF, defined as the ratio  
129 between  $\lambda\text{ET}$  and available energy, which is net radiation minus soil heat flux  $R_n - G$ ) and a consistent fraction  
130 (up to 3%) of the overall variability in European summer air temperature could be explained by  $f_{\text{diff}}$ . With  
131 increasing  $f_{\text{diff}}$ , the magnitude of the ET increase due to  $f_{\text{diff}}$  has been shown to be smaller than that of GPP,  
132 resulting in an increase in the ecosystem water use efficiency (WUE, defined as the ratio between GPP and ET)  
133 (Knobl and Baldocchi, 2008; Oliveira et al., 2011). Similarly to GPP, the local environment can also alter the  
134 responses of ecosystem ET, EF and WUE to  $f_{\text{diff}}$ . For instance, in temperature-limited ecosystems at high  
135 latitudes, incoming longwave radiation has been shown to be an important source of energy for snow and glacier  
136 melting under cloudy conditions with high  $f_{\text{diff}}$  increasing surface temperature (Juszak & Pellicciotti, 2013).  
137 However, the impacts of higher longwave radiation on the energy budget and canopy temperature have not been  
138 considered yet, despite their potentially important implications for vegetation activities. In general, compared to  
139 studies on evaluating impacts of  $f_{\text{diff}}$  on GPP and LUE, studies on the influence of  $f_{\text{diff}}$  on ET, EF and WUE are  
140 limited. More studies are needed to quantify impacts and understand mechanisms linking  $f_{\text{diff}}$  to ET, EF and  
141 WUE.

142 Traditionally, models that incorporate satellite remotely sensed observations, e.g. vegetation indices, surface  
143 temperature or albedo, to estimate GPP and ET, tend to be biased to clear sky conditions, due to lack of  
144 representation of cloudy conditions. These remote sensing models estimating GPP and ET can be classified into

145 ‘top-down’ and ‘bottom-up’ approaches (Houborg et al., 2009). ‘Top-down’ methods, e.g. CASA (Potter et al.,  
146 1993), the MODIS GPP and ET algorithms (Running et al., 2004; Mu et al., 2007) or the Priestley–Taylor Jet  
147 Propulsion Laboratory (PT-JPL) ET model (Fisher et al., 2008; Garcia et al., 2013), are simpler and can be  
148 directly driven with remote sensing variables. These models try to represent the ecological behavior of the  
149 canopy as a whole, using effective variables and few parameters. ‘Top-down’ models generally estimate GPP  
150 and ET assuming that the maximum LUE ( $\epsilon_{\max}$ ) of plant canopies and the maximum ET are constrained by  
151 similar stress-constraints reflecting different environmental constraints (Leuning et al., 1995; Houborg and  
152 Soegaard, 2004; Houborg et al., 2009; Garcia et al., 2013). ‘Top-down’ GPP approaches, have the advantage that  
153 forcing variables, such as the fraction of absorbed PAR at the top of the canopy or the land surface temperature,  
154 can be routinely estimated from remote sensing data instead of using a detailed description of canopy profiles  
155 and leaf energy budgets as in ‘bottom-up’ methods (Wang and Leuning, 1998; Ryu et al., 2011). Due to the  
156 impacts on the overall ecosystem GPP and ET, ‘top-down’ approaches can also benefit from considering  $f_{\text{diff}}$ . For  
157 instance, Yuan et al. (2014) found six of the seven LUE GPP models, which did not consider  $f_{\text{diff}}$ , significantly  
158 underestimated GPP during cloudy days. Recent studies incorporated the sunlit and shaded leaf approach into the  
159 MODIS LUE algorithm to improve satellite based GPP estimation (He et al., 2013; Zhou et al., 2015). Donohue  
160 et al. (2014) extended Roderick et al.’s (2001) LUE formulation to include the dependency of  $\epsilon_{\max}$  on  $f_{\text{diff}}$  and on  
161 the light-saturated rate of photosynthesis at the top of the canopy, yielding a highly generic model that accurately  
162 predicted GPP across Australia. Wang et al. (2015) added the information of cloudiness index (CI) to improve  
163 MODIS LUE algorithm. However, for ‘top-down’ ET models e.g. the Priestley Taylor based PT-JPL ET model,  
164 the effects of  $f_{\text{diff}}$  have not been investigated previously. Furthermore, it has not been investigated, whether or not  
165 the same set of biophysical constraints can be used to down-regulate both GPP and ET.

166 The outputs of ‘top-down’ models can be evaluated against eddy covariance (EC) datasets, including carbon and  
167 water fluxes between the land surface and the atmosphere at the ecosystem scale. Long-term eddy covariance  
168 and micrometeorological observations are also important to assess the environmental controls of carbon and  
169 water exchange (Baldocchi et al., 2003) using statistical approaches, e.g. path analysis (Bassow & Bazzaz, 1998;  
170 Huxman et al., 2003; Wu et al., 2016). In this study, we used a an 11-year time series of EC observations, a joint  
171 GPP and ET ‘top-down’ model and in-situ sap flow observations from a high latitude temperate deciduous forest  
172 ecosystem at Soroe in Denmark, to assess the impacts of  $f_{\text{diff}}$  on GPP and ET. At this site, 73.54% of all days are  
173 non-clear ( $f_{\text{diff}} > 50\%$ ). This percentage is higher than the global average level (ca. 50%, Kanniah et al., 2012).  
174 The specific objectives are: (1) to evaluate how  $f_{\text{diff}}$  independently and jointly with other biophysical constraints  
175 affects daily carbon and water fluxes in a deciduous forest; (2) to incorporate  $f_{\text{diff}}$  as a biophysical constraint into  
176 remote sensing based ‘top-down’ models to improve GPP and ET simulations. This study provides insights on  
177 the relative contribution of  $f_{\text{diff}}$  to the total variability on daily carbon and water fluxes encountered over multiple  
178 years using both statistical path analysis and global sensitivity analysis of ‘top-down’ models. It also explores  
179 potential mechanisms increasing LUE, WUE and evaporative fraction (EF) under diffuse conditions for high  
180 latitude ecosystems.

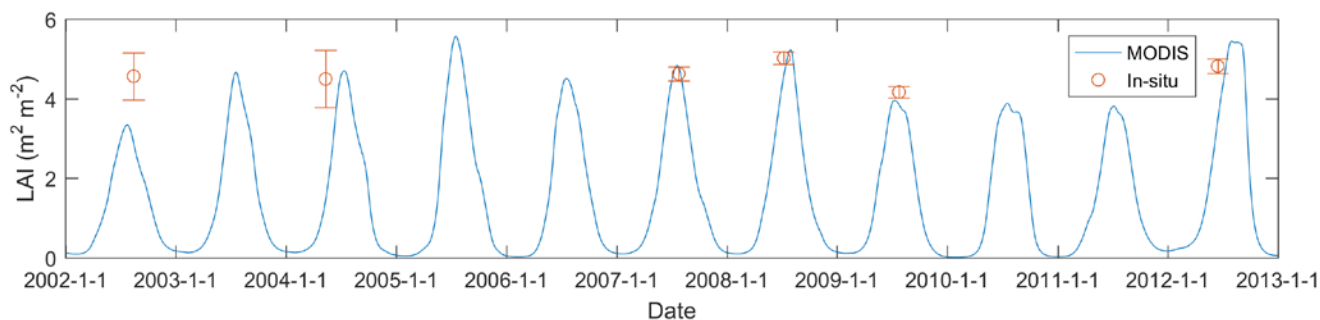
181

## 182 2. Study site and data

183 A Danish temperate deciduous beech forest site (Soroe on Zealand, Denmark, 55°29’N, 11°38’E) has been  
184 selected to evaluate the impacts of  $f_{\text{diff}}$  on the ecosystem carbon and water fluxes. The Soroe flux site has long-

185 term records of eddy covariance fluxes since 1996, diffuse / total PAR measurements during the period from  
186 2004 to 2013, and sap flow data from 2009 to 2011. The mean annual precipitation is 564 mm and the mean  
187 annual temperature is 8.5 °C. The dominant tree species is European beech (*Fagus sylvatica* L.) with  
188 approximately 20% conifers, mainly Norway spruce (*Picea abies* (L.) Karst.) and European larch (*Larix decidua*  
189 (Mill.)) (Wu et al., 2013). Leaf area index (LAI) peaks at 4-5 m<sup>2</sup>·m<sup>-2</sup>. Soil was classified as Alfisols or Mollisols  
190 with 10-40 cm deep organic layers. Details of this site are reported in Pilegaard et al. (2001) and Pilegaard et al.  
191 (2011).

192 Eddy covariance and micrometeorological observations and satellite data from the Moderate Resolution Imaging  
193 Spectroradiometer (MODIS) onboard of TERRA were used. The diffuse and total incoming PAR were measured  
194 by the Delta-T BF3 sensor. Eddy covariance and micrometeorological observations include GPP, ET, Rn-G,  
195 incoming longwave radiation (LW<sub>in</sub>), outgoing longwave radiation (LW<sub>out</sub>) and incoming shortwave radiation  
196 (SW<sub>in</sub>), air temperature (Ta), vapor pressure deficit (VPD) and soil water content (SWC). More details on this  
197 dataset can be found in Wu et al. (2012). The initial half-hourly observations were downloaded from the Fluxnet  
198 database (<https://fluxnet.ornl.gov/>), filtered by quality control flags and energy closure errors, and aggregated  
199 into daily values. Flag quality controlled GPP and ET observations spanning the period from 2002 to 2012 were  
200 used for analysis and modeling. For ET, observations with negative sensible heat flux, latent heat flux and net  
201 radiation were further excluded. Sap flow data were measured continuously for six beech trees during the period  
202 of 2009-2011 using the stem-heat balance technique (Granier et al., 1985). Averaged data from these six trees  
203 were used to represent the ecosystem-scale transpiration and to evaluate the simulated transpiration. Due to  
204 technical issues, there were gaps in the sap flow data. The daily ecosystem scale transpiration was only  
205 calculated, if more than three tree observations per day are available. Normalized difference vegetation index  
206 (NDVI) from the MODIS satellite vegetation index product (MOD13Q1, 16 day composite at 250m resolution  
207 L3 product, <https://reverb.echo.nasa.gov/>) was downloaded to infer the vegetation phenology and to retrieve LAI  
208 dynamics from 2002 to 2012. The initial 16-day synthetic data were further smoothed by the Savitzky–Golay  
209 filter in order to reduce the impacts of clouds and then interpolated into daily data by the spline algorithm (Chen  
210 et al., 2004). Further, LAI was obtained from NDVI by the locally empirical relationship  
211  $LAI = 0.001306e^{9.241NDVI}$  from Boegh et al. (2009). Both LAI from MODIS and in-situ measurements by LAI-  
212 2200C Plant Canopy Analyzer (LI-COR Inc., Lincoln, NE, USA) were shown in Figure 1. In general, LAI from  
213 MODIS NDVI captured the seasonal dynamics of vegetation. The peak values are 4-5.5 m<sup>2</sup>·m<sup>-2</sup> and these match  
214 the in-situ measurements and previous studies (Pilegaard et al. 2011; Wu et al., 2013).



215

216 Figure 1. The seasonal variation of LAI derived from MODIS NDVI in Soroe from 2002 to 2012 (continuous  
217 line). Dots are in-situ LAI measurements from LAI-2200C and the error bar shows the standard deviation.

218 Surface temperature,  $T_s$ , was calculated from in-situ incoming and outgoing longwave radiation based on the  
 219 Stefan–Boltzmann law, as in Eq. (1). The surface emissivity was estimated from NDVI (Van de Griend and Owe,  
 220 1993, Eq. 2).

$$221 \quad \varepsilon \cdot \sigma \cdot T_s^4 = LW_{\text{out}} - (1 - \varepsilon) \cdot LW_{\text{in}} \quad (\text{Eq. 1})$$

$$222 \quad \varepsilon = \begin{cases} 0.986 & (\text{NDVI} > 0.608) \\ 1.0094 + 0.047 \cdot \ln(\text{NDVI}) & (0.131 < \text{NDVI} < 0.608) \\ 0.914 & (\text{NDVI} < 0.131) \end{cases} \quad (\text{Eq. 2})$$

223 Where  $LW_{\text{out}}$  is longwave outgoing,  $LW_{\text{in}}$  is longwave incoming.  $\varepsilon$  is the surface emissivity and  $\sigma$  is the Stefan-  
 224 Boltzmann constant ( $5.670367 \times 10^{-8} \text{ kg} \cdot \text{s}^{-3} \cdot \text{K}^{-4}$ ). NDVI is from MODIS products. 0.986 is emissivity for dense  
 225 vegetation ( $\text{NDVI} > 0.608$ ) and 0.914 is emissivity for bare soil ( $\text{NDVI} < 0.131$ ).

226  $f_{\text{diff}}$  is the ratio between the observed diffuse PAR and the total PAR at the ground (Table 1). It is highly  
 227 correlated with the atmospheric transmission. Several indices could be used to infer  $f_{\text{diff}}$  (Butt et al., 2010).  
 228 Among them, the cloudiness index (CI), which is one minus the ratio between the observed PAR at ground and  
 229 PAR at the top of atmosphere (TOA) (Table 1), was often used to represent  $f_{\text{diff}}$  (Orgill and Hollands, 1977; Butt  
 230 et al., 2010; Wang et al., 2015). The advantage of CI is that it only requires one measurement, the total PAR at  
 231 the surface. The PAR at TOA could be calculated based on the time and the location on the Earth. In order to  
 232 determine  $f_{\text{diff}}$ , ground measurements of both diffuse and total PAR are required. The CI approach was more  
 233 favorable to be used in places without total and diffuse PAR measurements. In order to make this study more  
 234 applicable for other regions, CI was adopted as a proxy of  $f_{\text{diff}}$  to assess its impacts on carbon and water exchange.  
 235 Additionally in our data set,  $f_{\text{diff}}$  is available from 2004, while CI has a longer time series since 2002. To identify  
 236 the difference between CI and  $f_{\text{diff}}$ , these two indices were compared through statistical correlation and modeling  
 237 tests.

238

### 239 3. Methods

240 First, statistical analysis was conducted for in-situ eddy covariance and micrometeorological variables from 2002  
 241 to 2012 to identify the relationship between CI (a proxy for  $f_{\text{diff}}$ ) and observed daily GPP, ET, LUE, EF and  
 242 WUE. Then, a joint GPP and ET ‘top-down’ parsimonious model was used to simulate daily GPP and ET. The  
 243 model is based on the remote sensing LUE GPP model (Potter et al., 1993; Monteith et al., 1972) and Priestley–  
 244 Taylor Jet Propulsion Laboratory ET model (PT-JPL, Fisher et al., 2008). In this model, the same biophysical  
 245 constraints were used to reduce GPP and ET from potential to actual values. Model accuracy was compared for  
 246 the cases with and without considering CI. A global sensitivity analysis (GSA, Saltelli et al., 2010) was used to  
 247 quantify the sensitivity of GPP and ET to  $f_{\text{diff}}$ . Both statistical analysis and model based GSA provide estimates  
 248 of the independent and joint effects of CI on environmental variables. Their results were compared in order to  
 249 thoroughly understand effects of CI and related meteorological variables on the carbon and water exchange.  
 250 Finally, to check the difference between CI and  $f_{\text{diff}}$ , these two indices were compared through statistical analysis  
 251 and modeling tests.

### 252 3.1 Statistical analysis

253 To qualitatively explore the responses of GPP and ET to different levels of CI, relationships for GPP vs. PAR,  
254 ET vs. Rn-G, ET vs. PAR were analyzed under predominantly diffuse (CI>0.66) or direct (CI<0.33) radiation  
255 conditions. We chose 0.66 and 0.33 as thresholds to have equal intervals between 0 and 1, following the  
256 thresholds adopted in Davin and Seneviratne (2012). It has been shown in other ecosystems that CI can covariate  
257 with vegetation phenology obscuring the actual contribution of CI to GPP (Williams et al., 2016). To address  
258 that and control for the phenology effect on GPP and ET, we compared LUE, EF and WUE under diffuse or  
259 direct radiation conditions for different levels of NDVI, to make sure that they reflect the same phenological  
260 state. Afterwards, path analysis was used to quantitatively assess these relationships. These results informed  
261 parsimonious model design by identifying the most important drivers of GPP and ET in this ecosystem. The  
262 statistical tests were performed in a significance level of  $p<0.05$  ( $1.96 \times$ Standard Error).

263 Path analysis is a multiple regression technique that considers the covariance among variables. It is mainly used  
264 for variables that are highly correlated (Li, 1975) e.g. PAR, Ta and VPD. This method has been applied to  
265 evaluate environmental controls on carbon exchange in various ecosystems (Bassow & Bazzaz, 1998; Huxman  
266 et al., 2003; Wu et al., 2016). It assumes that the correlation between variable  $i$  and dependent variable  $y$  can be  
267 decomposed into direct and indirect effects. Where the direct effect means that input variable  $i$  directly affects  
268 output variable  $y$ . The direct value is also called path value and is the standardized partial regression coefficient.  
269 The indirect effects consider how variable  $i$  influences another variable  $j$  ( $j \neq i$ ) which in turn affects the output  $y$ .  
270 For example, a direct effect of CI on GPP will reflect the net change in GPP due to solely CI, while the rest of  
271 variables (e.g. PAR or air temperature) are fixed. However, the indirect effect will reflect how CI influences  
272 other environmental variables (e.g. PAR or air temperature) and in turn, these variables influence GPP. These  
273 direct and indirect effects represent the relative strength of a given relationship. Eq. 3 shows the formulas for this  
274 decomposition.

$$275 \quad r_{i,y} = r_{i,1}P_{1,y} + r_{i,2}P_{2,y} + \dots + r_{i,i}P_{i,y} + \dots + r_{i,n}P_{n,y} \quad (i=1, 2, 3, \dots, n) \text{ (Eq. 3)}$$

276 Where  $r_{i,y}$  is the correlation coefficient between input variable  $i$  and output  $y$ . It decomposes into the direct effect  
277  $P_{i,y}$  and indirect effects  $r_{i,n}P_{n,y}$  ( $n \neq i$ ).  $P_{i,y}$  is the direct effect from input variable  $i$  to output variable  $y$ .  $r_{i,n}$  is  
278 the correlation coefficient between the variable  $i$  and variable  $n$ .  $r_{i,n} * P_{n,y}$  ( $n \neq i$ ) are the indirect effects. The  
279 indirect effect quantifies the effect of one variable on another variable, which in turn affects the dependent  
280 variable.

281 To provide a quantitative assessment of the contribution of diffuse/direct PAR to the daily variability of carbon  
282 and water fluxes over 11 years and its interactions with other environmental variables, path analysis was  
283 performed considering the effect of various environmental factors on the target variables at the daily time scale  
284 from 2002 to 2012. Besides CI, environmental factors include Ta, PAR, Rn-G, LAI, VPD and SWC. Target  
285 variables are GPP,  $\lambda$ ET, LUE, EF and WUE.

286

287 3.2 Joint Gross Primary Productivity and Evapotranspiration model

288 To simulate the effects of  $f_{diff}$  on GPP and ET, a joint LUE GPP and PT-JPL ET model was used. Both  
 289 approaches estimate GPP or ET under potential conditions and then the potential values are down-regulated by  
 290 the same biophysical constraints reflecting multiple limitations or stresses. These constraints can be derived from  
 291 remote sensing and atmospheric data (McCallum et al., 2009; Garcia et al, 2013). The LUE GPP model is  
 292 recognized as a robust method to estimate GPP across various ecosystems and climate regimes (McCallum et al.,  
 293 2009). The PT-JPL ET model has been demonstrated as one of best-performing global remote sensing ET  
 294 algorithms in multi-algorithm inter-comparisons (Chen et al., 2014; Ershadi et al., 2014; Vinukollu, Meynadier  
 295 et al., 2011; Vinukollu, Wood et al., 2011; Michel et al., 2016; Miralles et al., 2016). Therefore, these two ‘top-  
 296 down’ GPP and ET models were selected for this study.

297 Most widely used LUE models e.g. CASA (Potter et al., 1993) or the MODIS algorithm (Running et al., 2004)  
 298 are based on the assumption that plants optimize canopy LUE or whole canopy carbon gain per total PAR  
 299 absorbed (Monteith et al., 1972). They have common features to estimate GPP: (1) ecosystem GPP is directly  
 300 related to absorbed PAR (APAR) through LUE, and (2) LUE may be reduced below its theoretical potential  
 301 value by environmental stresses such as low temperature or water shortage (Landsberg, 1986). The general form  
 302 of the LUE GPP model used in this study is shown in Eq. (4) and it is partly based on the Carnegie-Ames-  
 303 Stanford-Approach (Potter et al., 1993) with improvements by including constraints to account for fraction of the  
 304 canopy that is photosynthetically active vegetation (Fisher et al., 2008).

305 
$$GPP = \varepsilon_{max} \cdot PAR_c \cdot f_g \cdot f_M \cdot f_{Ta} \cdot f_{VPD} \cdot f_{SWC} \quad \text{Eq. (4)}$$

306 Where GPP is the gross primary productivity ( $\text{g}\cdot\text{C}\cdot\text{m}^{-2}\cdot\text{d}^{-1}$ ).  $\varepsilon_{max}$  is the maximum LUE ( $\text{g}\cdot\text{C}\cdot\text{MJ}^{-1}$ ).  $PAR_c$  is the  
 307 daily photosynthetically active radiation (PAR) ( $\text{MJ}\cdot\text{m}^{-2}\cdot\text{d}^{-1}$ ) intercepted by the canopy and it is calculated based  
 308 on the extinction of PAR within the canopy using the Beer Lambert law (Table 1).  $f_g$  is the green canopy  
 309 fraction indicating the proportion of active canopy.  $f_M$  is the plant moisture constraint.  $f_{Ta}$  is the air temperature  
 310 constraint reflecting the temperature limitation of photosynthesis.  $f_{VPD}$  is the VPD constraint reflecting the  
 311 stomatal response to the atmospheric water saturation deficit.  $f_{SWC}$  is the soil moisture constraint on  
 312 photosynthesis. All these constraints range from 0 and 1 and represent the reduction of maximum GPP under  
 313 limiting environmental conditions. For more details, see Table 1 and Fisher et al., (2008).

314 The Priestley-Taylor Jet Propulsion Laboratory model (PT-JPL, Fisher et al., 2008) is based on the Priestley and  
 315 Taylor (1972) equation for potential evapotranspiration, and incorporates eco-physiological variables to down-  
 316 regulate potential evapotranspiration to actual evapotranspiration. PT-JPL is a three source evapotranspiration  
 317 model, which includes wet surface evaporation (Ei), transpiration (Ec) and soil evaporation (Es), as described in  
 318 equations (5-8).

319 
$$\lambda ET = \lambda Ei + \lambda Ec + \lambda Es \quad \text{Eq. (5)}$$

320 
$$\lambda Ei = f_{wet} \cdot \alpha \Delta / (\Delta + \gamma) \cdot R_{nc} \quad \text{Eq. (6)}$$

321 
$$\lambda Ec = (1 - f_{wet}) \cdot f_g \cdot f_M \cdot f_{Ta} \cdot \alpha_c \Delta / (\Delta + \gamma) \cdot R_{nc} \quad \text{Eq. (7)}$$

322 
$$\lambda Es = f_{SWC} \cdot \alpha \Delta / (\Delta + \gamma) \cdot (R_{ns} - G) \quad \text{Eq. (8)}$$

323 Where  $\lambda ET$  is the latent heat flux for total evapotranspiration ( $W \cdot m^{-2}$ ),  $\lambda Ei$  is evaporation of intercepted water  
324 ( $W \cdot m^{-2}$ ),  $\lambda Ec$  is transpiration ( $W \cdot m^{-2}$ ), and  $\lambda Es$  is evaporation of soil water ( $W \cdot m^{-2}$ ). The quantity  $f_{wet}$  is the  
325 relative surface wetness to partition the evapotranspiration from the intercepted water and canopy transpiration  
326 (Fisher et al., 2008). The symbols  $f_g$ ,  $f_M$ ,  $f_{Ta}$  and  $f_{SWC}$  denote biophysical constraints and have the same  
327 meaning as in Eq. 4.  $f_{wet}$  They vary from 0 to 1 to account for the relative reduction of potential  $\lambda ET$  under  
328 limiting environmental conditions.  $R_{nc}$  and  $R_{ns}$  are the net radiation for canopy and soil, respectively. The  
329 partitioning of PAR and net radiation between canopy and soil is calculated following the Beer-Lambert law  
330 (Table 1).  $G$  is the ground heat flux.  $\Delta$  is the slope of saturation-to-vapor pressure curve.  $\gamma$  is the psychrometric  
331 constant.  $\alpha$  is an empirical ratio of potential evapotranspiration to equilibrium potential evapotranspiration (PT  
332 coefficient) replacing the atmospheric demand and surface resistance effects in the Penman-Monteith ET  
333 equation. Here for  $\lambda Ei$  and  $\lambda Es$ ,  $\alpha$  is equal to 1.26. This is also the suggested value for the PT-JPL model (Fisher  
334 et al., 2008).  $\alpha_c$  is the coefficient for  $\lambda Ec$  and it is the only parameter in the model that requires calibration.

335 In order to make the models parsimonious and robust, only those constraints/variables having significant  
336 relationships with GPP and  $\lambda ET$  were included in the LUE and PT-JPL models. Table 1 shows the detailed  
337 information on the model constraints and parameters for LUE and PT-JPL models.

338 Table 1. Model parameters and equations.  $SZA$  is the sun zenith angle. The extinction coefficients for PAR ( $k_{PAR}$ )  
339 and for net radiation ( $k_{Rn}$ ) were equal to 0.5 and 0.6, respectively (Ross, 1976; Impens & Lemur, 1969; Fisher et  
340 al., 2008),  $RH$  is the relative humidity.

Parameter	Description	Equation	Reference
$f_g$	Green canopy fraction	$f_g = f_{APAR} / f_{IPAR}$	Fisher et al., 2008
$f_M$	Plant moisture constraint	$f_M = f_{APAR} / \max(f_{APAR})$	Fisher et al., 2008
$f_{Ta}$	Plant temperature constraint	$f_{Ta} = 1.1814 \cdot [1 + e^{0.3(-T_o - 10 + T_a)}]^{-1} [1 + e^{0.2(T_o - 10 - T_a)}]^{-1}$	Potter et al., 1993
$f_{SWC}$	Soil moisture constraint	$f_{SWC} = \frac{SWC - SWC_{\min}}{SWC_{\max} - SWC_{\min}}$	Fisher et al., 2008
$f_{VPD}$	Vapor pressure deficit constraint	$f_{VPD} = 1 / (1 + VPD / D_0)$	Lohammar et al., 1980
$f_{wet}$	Relative surface wetness	$f_{wet} = RH^4$	Fisher et al., 2008
$f_{ci}$	Cloudiness index constraint	$f_{ci} = 1 - \frac{CI - CI_{\min}}{CI_{\max} - CI_{\min}}$	This study
$f_{di}$	Fraction of diffuse PAR constraint	$f_{di} = \frac{f_{diff} - \min(f_{diff})}{\max(f_{diff}) - \min(f_{diff})}$	This study
PARc	PAR intercepted by the canopy	PARc = PAR - PARs	Ruimy et al., 1999
PARs	PAR for the soil	PARs = PAR $\cdot e^{\frac{-k_{PAR} \cdot LAI}{\cos(SZA)}}$	Ruimy et al., 1999
Rnc	Net radiation for the canopy	Rnc = Rn - Rns	Fisher et al., 2008
Rns	Net radiation for the soil	Rns = Rn $\cdot e^{\frac{-k_{Rn} \cdot LAI}{\cos(SZA)}}$	Fisher et al., 2008

LAI	Leaf area index	$LAI = 0.001306e^{9.241NDVI}$	Boegh et al., 2009
$f_{APAR}$	Fraction of PAR absorbed by green vegetation cover (SAVI: soil adjusted vegetation index)	$SAVI = 0.45 NDVI + 0.132$ $f_{APAR} = 1.4 SAVI - 0.05$	Fisher et al., 2008
$f_{IPAR}$	Fraction of PAR intercepted by total vegetation cover	$f_{IPAR} = 1.0 NDVI - 0.05$	Fisher et al., 2008
CI	Cloudiness index	$CI = 1 - PAR_{obs}/PAR_{TOA}$	Spitters et al., 1986
$f_{diff}$	Fraction of diffuse PAR	$f_{diff} = PAR_{diffuse}/PAR_{total}$	Spitters et al., 1986
To	Optimum plant growth temperature	Ta at $\max\{PAR \cdot f_{APAR} \cdot Ta/VPD\}$ 16.51 °C for this study	Fisher et al., 2008
D0	Empirical coefficient for VPD	15 hPa	Leuning et al., 1995

341

### 342 3.3 Incorporating diffuse fraction into the joint GPP and ET model

343 Previous studies have improved the LUE GPP models by considering the impacts of CI on LUE (e.g. Turner et al., 2006; Wang et al., 2015; Wu et al., 2016). For this study, we used a similar approach to modify Eq. (4) to incorporate the CI constraint into the GPP model, as Eq. (9). Moreover,  $\epsilon_{max}$  now represents the maximum LUE under totally diffuse radiation conditions instead of the maximum value for all sky conditions.

347 In the PT-JPL model, the PT coefficient ( $\alpha$ ) represents the atmospheric demand and the surface resistance for ET. Therefore, similar to the maximum LUE  $\epsilon_{max}$  in the GPP model, this study incorporated CI into ET via changes in the PT coefficient ( $\alpha_c$ ), which reflects the opening of stomata and stomatal conductance.

$$350 \quad GPP = (1 - \mu \cdot f_{ci}) \cdot \epsilon_{max} \cdot PAR_c \cdot f_g \cdot f_M \cdot f_{Ta} \cdot f_{VPD} \cdot f_{SWC} \quad \text{Eq. (9)}$$

$$351 \quad \lambda Ec = (1 - \tau \cdot f_{ci}) \cdot (1 - f_{wet}) \cdot f_g \cdot f_{Ta} \cdot f_M \cdot \alpha_c \Delta / (\Delta + \gamma) \cdot R_{nc} \quad \text{Eq. (10)}$$

352 Where  $f_g, f_M, f_{Ta}, f_{VPD}, f_{SWC}, f_{wet}$  have the same meaning as Eq. (2) and (7).  $PAR_c$  and  $R_{nc}$  are the PAR and Rn intercepted by the canopy, respectively.  $(1 - \mu \cdot f_{ci})$  and  $(1 - \tau \cdot f_{ci})$  are the subtractive formulas to represent the fraction of diffuse PAR constraints for GPP and ET, respectively.  $\mu$  indicates an overall sensitivity of GPP to CI.  $\tau$  reflects the sensitivity of  $\lambda Ec$  to CI. In these approaches,  $f_{ci}$  can also be replaced by  $f_{di}$ , in order to drive the model with  $f_{diff}$  instead.

357

### 358 3.4 Model calibration and validation

359 The LUE GPP model version without considering diffuse light (Eq. 2) had only one parameter,  $\epsilon_{max}$  (maximum LUE) to be optimized or adjusted to the vegetation type. In the new diffuse/direct model version (Eq. 9), an additional parameter  $\mu$  (the sensitivity of GPP to CI) needs to be optimized as well. In the initial PT-JPL ET model (Eq. 7), the  $\alpha_c$  parameter was optimized, while in the modified PT-JPL ET model (Eq. 10),  $\tau$  (the

363 sensitivity of  $\lambda Ec$  to CI) needs to be optimized additionally. Table 2 shows the details on these calibrated  
 364 parameters.

365 Table 2. The calibrated parameters for the joint GPP and ET model

Models	Parameter	Without CI (Eq. 4 and 7)	With CI (Eq. 9 and 10)	Range	Optimized value (Without CI / with CI)
GPP	$\varepsilon_{max}$	Maximum LUE ( $\text{g}\cdot\text{C}\cdot\text{m}^{-2}\cdot\text{MJ}^{-1}$ )	Maximum LUE under total diffuse PAR conditions ( $\text{g}\cdot\text{C}\cdot\text{m}^{-2}\cdot\text{MJ}^{-1}$ )	0~5	2.97 / 4.29
	$\mu$		GPP sensitivity to $f_{CI}$ (dimensionless)	-1~1	0.46
ET	$\alpha_c$	PT coefficient for the canopy (dimensionless)	PT coefficient for the canopy under total diffuse PAR conditions (dimensionless)	1~3	1.32 / 2.60
	$\tau$		$\lambda Ec$ sensitivity to $f_{CI}$ (dimensionless)	-1~1	0.65

366  
 367 The Monte Carlo method was used to optimize these model parameters, with RMSE (root mean square error) as  
 368 the objective function. The parameter values were sampled 20,000 times with uniform distribution within their  
 369 corresponding ranges and these 20,000 parameter sets were used to run models. Odd years were used for  
 370 calibration and even years were for validation. The best-fit parameter set was chosen.

371 To compare model simulation performances with and without CI information, the Root Mean Square Error  
 372 (RMSE, Eq. 11), Correlation Coefficient (R, Eq. 12), Bias (Eq. 13), unbiased Root Mean Square Error (ubRMSE,  
 373 Eq. 14) and Standard Deviation (STD, Eq. 15) were used. Taylor diagrams (Taylor, 2001), were used to present  
 374 these three complementary statistics CC, Normalized STD (NSTD, as Eq. 16) and Normalized ubRMSE  
 375 (NubRMSE), which have a triangle-cosine-law-like relationship, as Eq. (17). The radial distance stands for the  
 376 NSTD and the angle in the polar plot represents R. The reference point located on the X-axis with R=1, NSTD=1  
 377 and NubRMSE=0 is the observation. The distance from the simulation point to the reference point means the  
 378 NubRMSE of simulations and it is the integrated performance for the simulation.

379 
$$\text{RMSE} = \sqrt{\sum_{i=1}^N (\text{sim}_i - \text{obs}_i)^2 / N} \quad (11)$$

380 
$$R = \frac{\sum_{i=1}^N (\text{sim}_i - \overline{\text{sim}})(\text{obs}_i - \overline{\text{obs}})}{\sqrt{\sum_{i=1}^N (\text{sim}_i - \overline{\text{sim}})^2} \times \sqrt{\sum_{i=1}^N (\text{obs}_i - \overline{\text{obs}})^2}} \quad (12)$$

381 
$$\text{BIAS} = \sum_{i=1}^N (\text{sim}_i - \text{obs}_i) / N \quad (13)$$

382 
$$\text{ubRMSE} = \sqrt{\sum_{i=1}^N [(\text{sim}_i - \overline{\text{sim}}) - (\text{obs}_i - \overline{\text{obs}})]^2 / N} \quad (14)$$

383 
$$\text{STD} = \sqrt{\sum_{i=1}^N (\text{sim} - \overline{\text{sim}})^2 / N} \quad (15)$$

384 
$$\text{NSTD}_{\text{sim}} = \text{STD}_{\text{sim}} / \text{STD}_{\text{obs}} \quad (16)$$

385 
$$\text{NubRMSE}_{\text{obs,sim}}^2 = \text{NSTD}_{\text{obs}}^2 + \text{NSTD}_{\text{sim}}^2 - 2\text{NSTD}_{\text{obs}}\text{NSTD}_{\text{sim}} \cos \text{CC}_{\text{obs,sim}} \quad (17)$$

386 Where  $\overline{sim}$  is the simulation,  $\overline{obs}$  is the observation,  $N$  is the total number,  $\overline{sim}$  is the average of the simulation,  
387 and  $\overline{obs}$  is the average of the observation.

388

### 389 3.5 Global sensitivity analysis

390 The Sobol' method (Sobol' et al., 1990) is one of the most commonly used global sensitivity analysis (GSA)  
391 methods. It is based on ANOVA (analysis of variance) decomposition and it allows calculating the sensitivity of  
392 coupled input forcing. The Sobol' method provides not only the first order sensitivity for each forcing factor but  
393 can also quantify interactions among forcing factors. The first order sensitivity quantifies the independent  
394 contribution from each forcing to the output variable, while the second order quantifies the interactions between  
395 each two forcing factors to the output variable. In our study, we aimed to identify the sensitivity of GPP and  $\lambda ET$   
396 to  $f_{ci}$ , in relation with other major environmental variables and assess if the model approach could pick the same  
397 sensitivities embedded in the dataset that will be captured by the path analysis. The variances of the terms in the  
398 ANOVA decomposition are estimated the following equations (Saltelli et al., 2010):

$$399 \quad V(Y) = \sum_{i=1}^n V_i + \sum_{i \leq j} V_{ij} + \dots + \sum_{1 \leq \dots \leq n} V_{1\dots n} \quad (18)$$

400 Where  $V_i$  represents the first order effect for each factor  $X_i$ ;  $V_{ij}$  stands for the second order effect for  $X_i, X_j$ ; and  
401  $V_{1\dots n}$  is the  $n^{\text{th}}$  order effect for  $X_1, \dots, X_n$ .

402 The first order sensitivity index  $S_i$  can be calculated by

$$403 \quad S_i = V_i/V(Y) = V[E(Y | X_i)]/V(Y) \quad (19)$$

404 And the second-order sensitivity index  $S_{ij}$  can be calculated by

$$405 \quad S_{ij} = V_{ij}/V(Y) = (V[E(Y | X_i, X_j)] - V_i - V_j)/V(Y) \quad (20)$$

406 In general, the total sensitivity index can be defined as:

$$407 \quad S_i^{\text{tot}} = E(V(Y|X_{\sim i}))/V(Y) \quad (21)$$

408 Where  $S$  stands for different order sensitivity index,  $V$  means the variance for different variables,  $E$  is the  
409 expectation, and  $\sim i$  refers to all of the inputs except input  $i$ .

410 The kernel density sampling method was applied to sample the input data set for sensitivity analysis. The  
411 advantage to use the kernel density sampling method is that it could resemble the distribution of sampled data set.  
412 According to the kernel density distribution of each model input, 20,000 samples will be generated to assess the  
413 model input sensitivity.

414

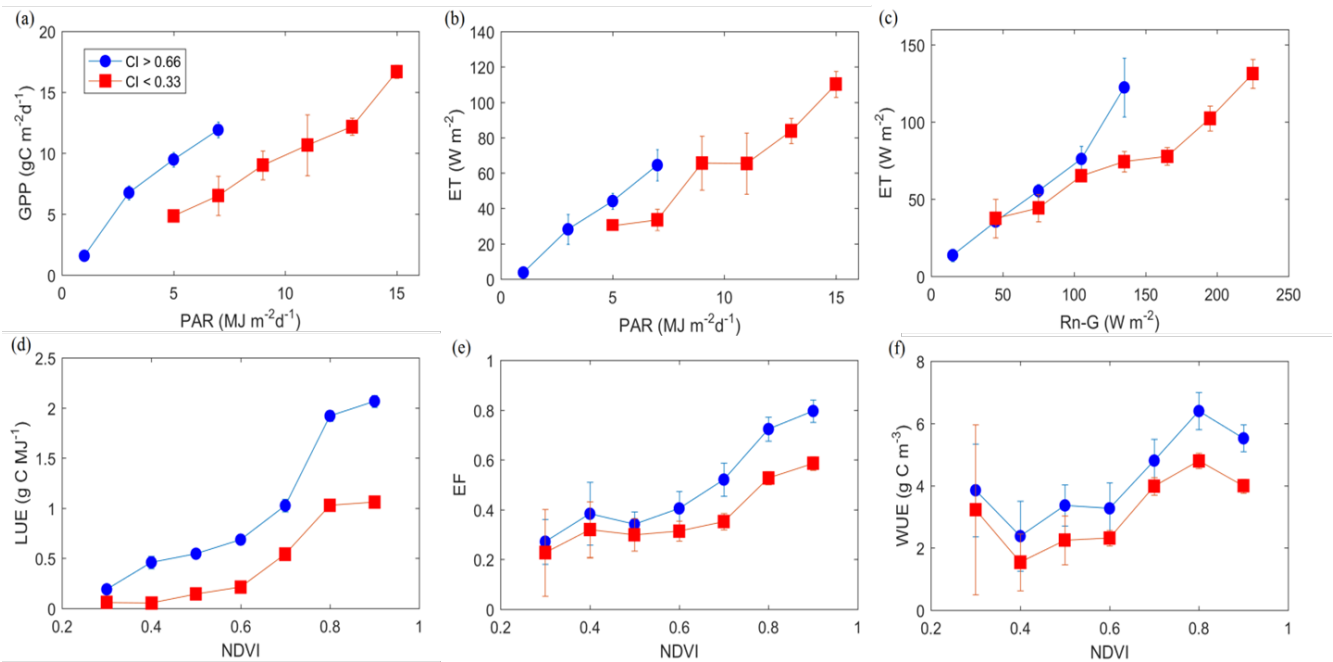
## 415 4. Results and discussion

### 416 4.1 Statistical analysis

417 First, we explored responses of daily GPP and  $\lambda$ ET to diffuse/direct radiation conditions while controlling for  
418 radiation levels. Daily GPP and  $\lambda$ ET from the eddy covariance flux tower were compared between  
419 predominately diffuse PAR conditions ( $CI>0.66$ ) and predominately direct PAR conditions ( $CI<0.33$ ) over the  
420 period from 2002 to 2012. Direct comparison for diffuse and direct radiation conditions could involve data from  
421 different days of the year with different phenology conditions and this comparison could exaggerate the actual  
422 diffuse fertilization effects (Williams et al., 2016). In order to compare the responses of daily GPP and  $\lambda$ ET with  
423 the phenology background, comparison in Figure 2 (a-c) was conducted with NDVI more than 0.75. Figure 2 (a-  
424 c) shows the evolution of GPP and  $\lambda$ ET as a function of PAR and Rn-G with predominantly diffuse and direct  
425 PAR conditions, respectively. There is a clear distinction of the response of GPP to PAR between diffuse and  
426 direct PAR conditions. As shown in Figure 2 (a), with PAR increasing, GPP increased significantly in the diffuse  
427 PAR conditions, while GPP increased slowly in the direct PAR conditions. The slope of the response curve  
428 represents LUE. This suggests that LUE in the diffuse PAR is higher than that in the direct radiation. The  
429 evolution of  $\lambda$ ET as a function of PAR or Rn-G in diffuse and direct radiation conditions is shown in the Figure  
430 2 (b) and (c), respectively. Similar to the response of GPP,  $\lambda$ ET is higher under predominately diffuse PAR  
431 conditions for the same level of PAR or Rn-G. However, the increase in  $\lambda$ ET is less obvious than that in GPP  
432 and this leads to the increase of WUE. These results are in agreement with a study on a deciduous temperate  
433 forest ecosystem of central Germany, which found that the diffuse/direct radiation could increase the ecosystem  
434 WUE (Knohl and Baldocchi, 2008). The slope of the response curve in Figure 2 (c) represents the evaporative  
435 fraction (EF), the ratio of between  $\lambda$ ET and Rn-G. This suggests that under diffuse PAR, higher photosynthesis  
436 rates lead to higher  $\lambda$ ET and higher EF. It should be also noticed that the difference for response curves in  $\lambda$ ET  
437 vs. PAR is clearer than that in  $\lambda$ ET vs. Rn-G. PAR does not include the information on the longwave radiation,  
438 while Rn-G contains the longwave radiation components. That indicates that longwave radiation components  
439 induced the difference between  $\lambda$ ET vs. PAR and  $\lambda$ ET vs. Rn-G.

440 To further explore the responses of daily LUE, EF and WUE to diffuse/direct radiation conditions, LUE, EF and  
441 WUE were compared with various levels of NDVI under predominately diffuse and direct PAR conditions, as  
442 shown in Figure 2 (d-f). In general, there is a significant difference for the response curves of diffuse and direct  
443 PAR conditions in LUE, EF and WUE. This indicates the ecosystem responds differently to the diffuse and  
444 direct PAR conditions. With higher levels of NDVI, the difference of LUE, EF and WUE between  
445 predominately diffuse conditions and predominately direct radiation conditions becomes more significant. This  
446 indicates diffuse PAR has stronger effects in high NDVI conditions. This is in agreement with the findings that  
447 in the ecosystem with high LAI, the diffuse fertilization effects are stronger (Alton et al., 2007).

448



449

450 Figure 2. The response of daily GPP,  $\lambda$ ET, LUE, EF and WUE to diffuse and direct radiation conditions during  
 451 the period from 2002 to 2012. The thresholds for predominantly diffuse and direct conditions are defined as CI  
 452 above 0.66 and below 0.33, respectively. (a) GPP as a function of PAR for predominantly diffuse light condition  
 453 (CI>0.66) and predominantly direct light conditions (CI<0.33). (b)  $\lambda$ ET as a function of PAR for predominantly  
 454 diffuse and direct light conditions. (c)  $\lambda$ ET as a function of Rn-G for predominantly diffuse and direct conditions.  
 455 (d) LUE as a function of NDVI for predominantly diffuse and direct conditions. (e) EF as a function of NDVI  
 456 for predominantly diffuse and direct conditions. (f) WUE as a function of NDVI for predominantly diffuse and  
 457 direct conditions. The points represent the mean value for specific PAR interval and the error bar represent the  
 458 significance level at  $p < 0.05$  ( $1.96 \times$ Standard Error). To exclude the influence from phenology, comparison in (a-c)  
 459 were conducted with NDVI more than 0.75.

460

461 The results of the path analysis are shown in Table 3-5. Table 3 presents the total effects (correlation coefficients)  
 462 among these important variables. CI has positive correlation with LUE, EF, EF\* and WUE, while it negatively  
 463 correlates with GPP,  $\lambda$ ET and  $\lambda$ ET\*.  $\lambda$ ET\* and EF\* are the observations with LAI greater than 2 and VPD larger  
 464 than 3.5 hPa. LAI greater than 2 corresponds to the growing season, while VPD larger than 3.5 hPa is associated  
 465 with lack of precipitation and limited evaporation of intercepted water. Both Ta and LAI positively correlate  
 466 with GPP, LUE,  $\lambda$ ET,  $\lambda$ ET\*, EF, EF\* and WUE. PAR also has positive correlation with GPP, LUE and WUE.  
 467 Rn-G has positive correlations with  $\lambda$ ET,  $\lambda$ ET\* and EF. This indicates that the ecosystem dynamics are  
 468 controlled by temperature and radiation. During the growing season, there is a negative correlation between VPD  
 469 and EF\*, reflecting stomatal control of transpiration. This can be seen also in the negative correlation of VPD  
 470 with EF\*. Even though there are parts of the year when the ecosystem is water controlled, the overall dynamics  
 471 are controlled by energy and temperature. This is supported by the negative correlation of SWC with GPP, LUE,  
 472  $\lambda$ ET and EF. The relation is only positive during high VPD and growing season periods ( $\lambda$ ET\*). In water-limited

473 ecosystems or situations, EF usually has negative correlation with VPD while SWC positively correlates with  
 474 GPP, LUE,  $\lambda$ ET and EF.

475 Table 3. The total effects (correlation coefficients) from environmental factors to target variables

Total effects	CI	Ta	PAR	Rn-G	LAI	VPD	SWC
GPP	-0.47	0.78	0.84	/	0.84	0.72	-0.31
LUE	0.11	0.71	0.28	/	0.73	0.27	-0.36
$\lambda$ ET	-0.29	0.73	/	0.76	0.77	0.64	-0.26
$\lambda$ ET*	-0.21	0.15	/	0.68	0.34	0.29	0.25
EF	0.12	0.59	/	0.11	0.63	0.21	-0.31
EF*	0.44	0.12	/	-0.36	0.20	-0.19	0.09
WUE	0.08	0.25	0.04	-0.05	0.22	0.03	-0.20

476 ‘/’ means not the input for the correlation test.

477

478 The total effects were further decomposed into direct and indirect effects using path analysis. Table 4 shows the  
 479 direct effects of environmental variables on the target variables. GPP,  $\lambda$ ET and WUE are mainly controlled by  
 480 radiation (either PAR or Rn-G). Once normalizing for different radiation as in LUE or EF variables the most  
 481 important factor was Ta. CI had significant positive direct effects on all target variables GPP, LUE,  $\lambda$ ET, EF and  
 482 WUE. That means that an increase in CI while maintaining the rest of considered variables fixed will produce a  
 483 net increase in GPP, LUE, ET and EF. Based on this when incorporating CI into the models, we should consider  
 484 that CI will increase GPP and ET (see Eq. (9) and (10)). Considering the whole year, the effects of CI on GPP,  
 485 LUE and WUE are stronger than on  $\lambda$ ET and EF. It is possible that the effect of CI on transpiration is masked by  
 486 evaporation from soil and intercepted water, which are insensitive to CI. When considering  $\lambda$ ET\* and EF\*, to  
 487 minimize the effect of evaporation of intercepted water and soil water, CI had stronger direct effects. This agrees  
 488 with the land surface modeling results by Davin and Seneviratne (2012), which show that CI mainly influences  
 489 transpiration and has limited impacts on evaporation from the intercepted water and soil. This finding further  
 490 supports our modeling approach, which incorporates CI into the transpiration module only. Variables related to  
 491 light harvesting by canopies (PAR and LAI) were the dominant factors regulating GPP. The top soil moisture  
 492 (SWC) has very limited effects on GPP. For LUE, Ta was the important factor with a positive correlation, which  
 493 emphasizes the sensitivity of this ecosystem to temperature. After Ta, LAI had also a positive effect while VPD  
 494 reduced LUE. CI ranked as the fourth most important factor to influence LUE with a positive response. Similar  
 495 to GPP, SWC had very weak effects on LUE. It is possible that the deep rooting system of the beech forest  
 496 enables sufficient water supply even though water in the top soil is depleted (Wu et al., 2012). From these  
 497 findings, we can conclude that the GPP and LUE of this high latitude ecosystem are controlled by radiation and  
 498 temperature. For  $\lambda$ ET, CI had a weaker but still significant influence considering the whole year. As expected,  
 499 CI had stronger impacts on  $\lambda$ ET\* during the growing season and in periods of high VPD. When normalizing  $\lambda$ ET  
 500 by the available energy (Rn-G), Ta was the dominant factor with a positive effect on EF, followed by LAI and  
 501 SWC. During the growing season, CI became the major controlling factor for EF\*.

502 In our site, after accounting for energy, Ta and CI are the main factors to influence WUE. WUE increased in  
 503 response to increases in Ta and CI. This is different from water-limited ecosystems, where increases in Ta tend  
 504 to decrease WUE (Stroosnijder et al., 2012) and diffuse PAR tends to compensate for this effect (Gu et al., 2002;

505 Rocha et al., 2004). However, higher VPD reduces GPP, LUE and  $\lambda$ ET and EF due to the strong stomatal control.  
 506 These findings are helpful to refine parsimonious models for the simulation of GPP and ET. For instance, SWC  
 507 of the top soil could not be the necessary input for GPP simulation, since it has weak impacts on GPP.

508 Table 4. The direct effects from environmental factors to target variables

Direct effects	CI	Ta	PAR	Rn-G	LAI	VPD	SWC
GPP	0.19	0.07	0.82	/	0.44	-0.17	0.02
LUE	0.31	0.58	0.20	/	0.47	-0.42	-0.02
$\lambda$ ET	0.03	0.14	/	0.51	0.50	-0.05	0.11
$\lambda$ ET*	0.12	0.01	/	0.67	0.25	0.00	0.18
EF	0.02	0.70	/	-0.35	0.46	-0.30	0.08
EF*	0.25	0.23	/	-0.29	0.20	-0.14	0.22
WUE	0.32	0.30	0.76	-0.46	-0.12	-0.24	-0.20

509 ET\* and EF\* are for conditions (LAI > 2 and VPD > 3.5 hPa). '/' means not the input for path analysis.

510

511 The indirect effects describe how CI influences ecosystem carbon and water fluxes through other intermediate  
 512 environmental variables over the whole year or the growing season, as shown in Table 5. Over the year, CI  
 513 mainly interacts with variables related to the radiation transfer (PAR, Rn-G and LAI) to reduce GPP and  $\lambda$ ET,  
 514 respectively. After these radiation variables, Ta and VPD have been shown to deliver major indirect effects from  
 515 CI to GPP, LUE,  $\lambda$ ET and EF. Higher CI over the year decreases Ta, decreasing in turn LUE and EF, but CI also  
 516 reduces VPD, which has positive effects on LUE and EF. For WUE, the effects of CI mainly go through PAR,  
 517 Rn-G and VPD. It should be also noticed that the paths through SWC are very weak or not significant.

518 Table 5. The indirect effects from CI through other environmental factors to target variables

Indirect effects from CI via:	Ta	PAR	Rn-G	LAI	VPD	SWC
GPP	-0.02	-0.63	/	-0.12	0.11	0.00
LUE	-0.18	-0.16	/	-0.13	0.27	0.00
$\lambda$ ET	-0.03	/	-0.28	-	0.03	-
$\lambda$ ET*	0.00	/	-0.36	0.04	0.00	-
EF	-0.19	/	0.19	-0.05	0.15	-
EF*	-0.03	/	0.14	0.02	0.06	-
WUE	-0.06	0.28	-0.59	-	0.14	-0.01

519 ET\* and EF\* are for conditions (LAI > 2 and VPD > 3.5 hPa). '/' means not the input for path analysis; '-'  
 520 means the path analysis is not significant.

521

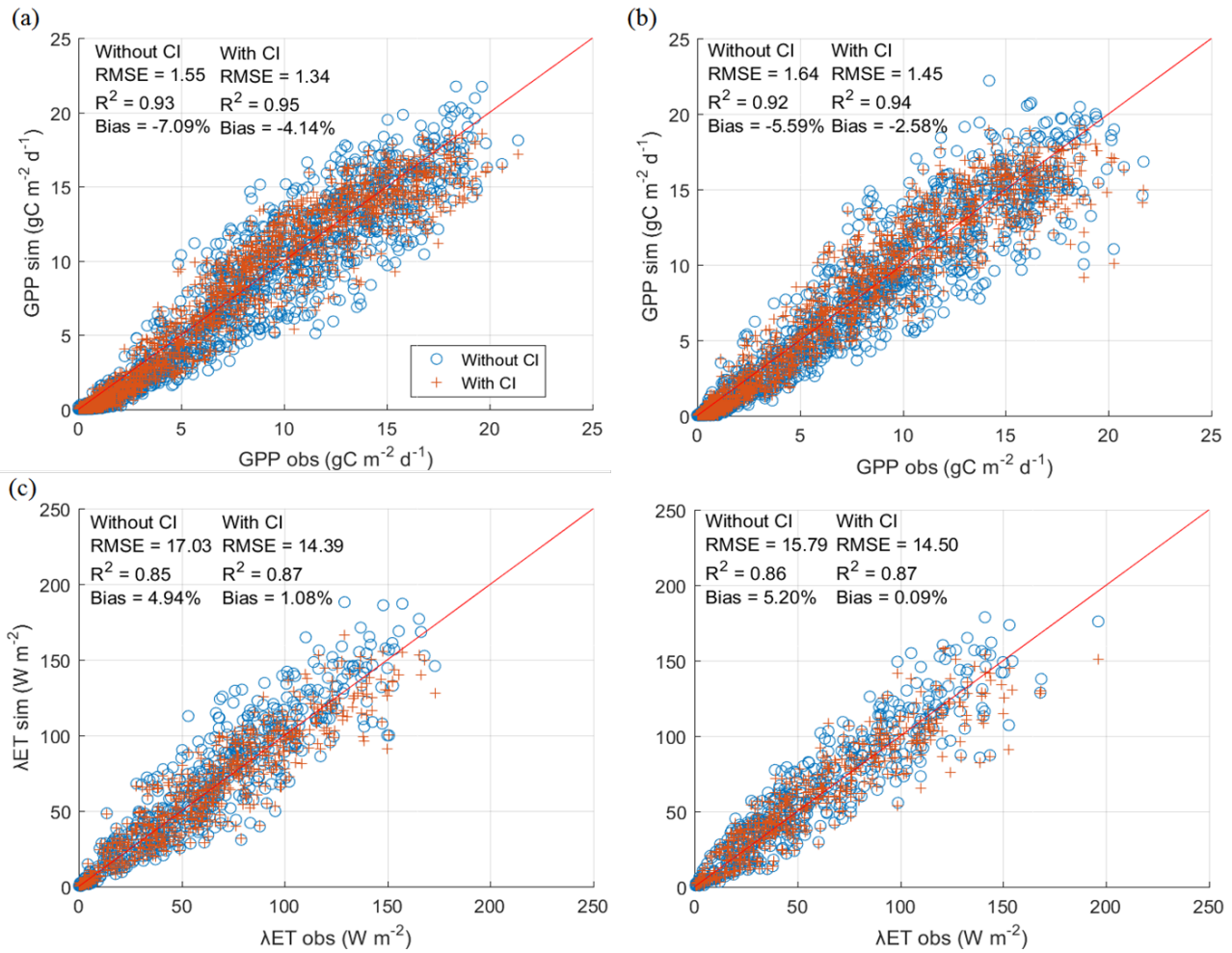
## 522 4.2 Joint Gross Primary Productivity and Evapotranspiration modeling

523 Based on path analysis, a parsimonious GPP and ET model was developed for the site. Since SWC was not a  
 524 significant factor influencing GPP in the path analysis, the soil moisture constraint was excluded in the GPP and  
 525 transpiration modeling but not for soil evaporation. The optimized parameter values increased, as shown in the  
 526 Table 2.  $\varepsilon_{max}$  increased from 2.97 to 4.29 and  $\alpha_c$  increased from 1.32 to 2.60. The increase of parameter values

527 is similar to that in Wang et al. (2015). In their study, CI was incorporated into the MODIS LUE algorithm and  
528 after optimization,  $\varepsilon_{\max}$  changed from 1.12 to 3.87 in a similar mixed deciduous broadleaf and evergreen needle  
529 forest as this study. The value of 2.60 for  $\alpha_c$  is also reasonable, considering for forests under totally diffuse  
530 radiation conditions. Depending on the land conditions,  $\alpha_c$  can reach a value of up to 3.62 in grass and forest  
531 (Lhomme, 1997).

532 The model performance of GPP and  $\lambda$ ET with and without CI was compared in Figure 3 during the calibration  
533 and validation periods. It can be seen that with CI, the skills of both GPP and ET models improved. During the  
534 calibration period, as shown in Figure 3 (a), RMSE of the simulated GPP decreased from 1.55 to 1.34  $\text{g}\cdot\text{C}\cdot\text{m}^{-2}\cdot\text{d}^{-1}$   
535 (RMSE reduced 13.25%).  $R^2$  increased from 0.93 to 0.95. Additionally, the bias was reduced from -7.09% to -  
536 4.14%. During the validation period, as shown in Figure 3 (b), RMSE of simulated GPP reduced from 1.64 to  
537 1.45  $\text{g}\cdot\text{C}\cdot\text{m}^{-2}\cdot\text{d}^{-1}$  (RMSE reduced 11.68%).  $R^2$  improved from 0.92 to 0.94. The bias changed from -5.59% to -  
538 2.58%. Further, we compared the improvement of the simulation performance between the whole period and the  
539 growing season. The RMSE of the simulated GPP during the whole period decreased from 1.59 to 1.39  $\text{g}\cdot\text{C}\cdot\text{m}^{-2}\cdot\text{d}^{-1}$   
540 (RMSE reduced 12.58%) and  $R^2$  increased from 0.93 to 0.94. While during the growing season, the RMSE  
541 dropped from 2.37 to 2.06  $\text{g}\cdot\text{C}\cdot\text{m}^{-2}\cdot\text{d}^{-1}$  (by 13.08%) and  $R^2$  increased from 0.68 to 0.73. It can be seen that there is  
542 more improvement in the growing season.

543 For  $\lambda$ ET, during the calibration period as shown in Figure 3 (c), when incorporating CI, the RMSE of simulated  
544  $\lambda$ ET from the PT-JPL model decreased from 17.03 to 14.39  $\text{W}\cdot\text{m}^{-2}$  (by 15.50%).  $R^2$  increased from 0.85 to 0.87.  
545 The bias was reduced from 4.94% to 1.08%. During the validation period, shown in Figure 3 (d), the RMSE was  
546 reduced from 15.79 to 14.50  $\text{W}\cdot\text{m}^{-2}$  (by 8.16%).  $R^2$  improved from 0.86 to 0.87, while the bias was reduced from  
547 5.20% to 0.09%. We also found for the whole period, the RMSE dropped from 16.09 to 14.44  $\text{W}\cdot\text{m}^{-2}$  (by  
548 10.25%), while during the growing seasons, the RMSE decreased from 19.08 to 16.89  $\text{W}\cdot\text{m}^{-2}$  (by 11.47%). Both  
549 GPP and  $\lambda$ ET simulation improves when incorporating CI into the models, especially during the growing season.  
550 The improvement of GPP simulations is more significant than that of  $\lambda$ ET. This agrees with the results from the  
551 statistical path analyses, which showed a higher effect of diffuse PAR on GPP than on  $\lambda$ ET. CI has stronger  
552 effects during the growing season ( $\lambda$ ET\*) than the effects during the whole period ( $\lambda$ ET). The higher sensitivity  
553 of GPP to  $f_{\text{diff}}$  than for  $\lambda$ ET has been also found in other studies (Mo and Liu, 2001; Knohl and Baldocchi, 2008;  
554 Oliveira et al., 2011).

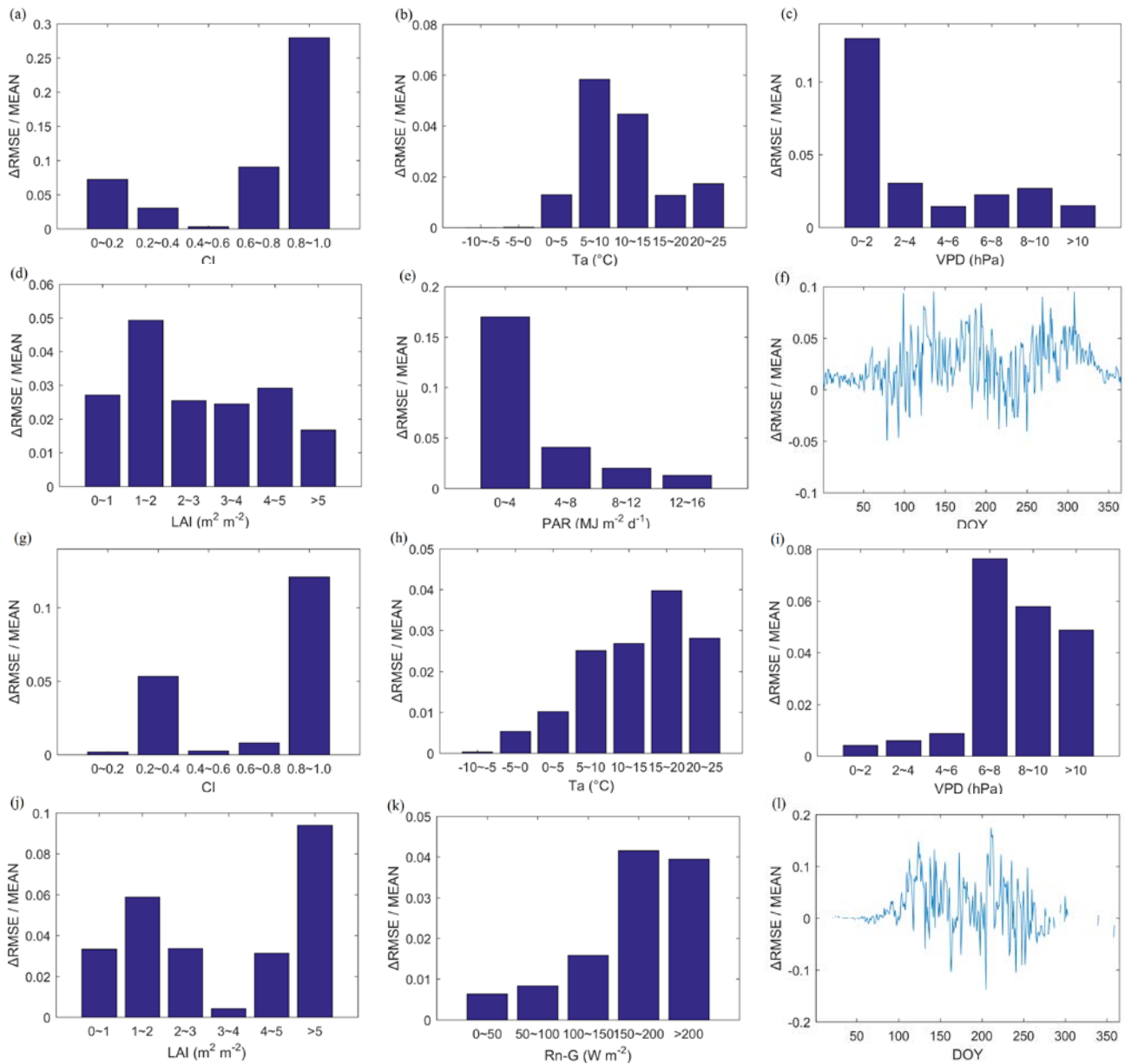


555

556 Figure 3. Scatter plots of the simulated and observed GPP (a: calibration, b: validation) and  $\lambda$ ET (c: calibration,  
 557 d: validation). The red dots are simulation with CI and the blue circles are the simulation without CI.

558 To understand under which environmental conditions there is a larger improvement of simulation performance,  
 559 we stratified the improvement in model errors,  $\Delta$ RSME / MEAN, by levels of CI, Ta, VPD, LAI, PAR or Rn-G,  
 560 and also assessed the effect of phenology by considering the day of the year (Figure 4).  $\Delta$ RSME is equal to  
 561  $RSME_{\text{without CI}} - RMSE_{\text{with CI}}$ . For different levels of CI, the RMSE for both GPP and  $\lambda$ ET simulation decreased  
 562 after including CI (Figure 4 (a) and (g)) with larger improvements for extreme CI values (e.g. sunny or  
 563 completely overcast). While for median CI conditions, the improvement is lower. This is because in the  
 564 simulation without CI, the optimized  $\varepsilon_{max}$  (Eq. 4) and  $\alpha_c$  (Eq. 7) tend to represent median CI conditions, as a  
 565 compromise that tends to be low in high diffuse fraction conditions and high in low diffuse fraction conditions.  
 566 In the simulation with CI,  $\varepsilon_{max}$  (Eq. 9) and  $\alpha$  (Eq. 10) were parameterized with CI and the simulation performs  
 567 well in high and low diffuse radiation conditions. As for temperature shown in Figure 4 (b) and (h), under low  
 568 temperatures the model improvements when incorporating CI are lowest, since both  $\lambda$ ET and GPP are low. For  
 569 VPD, both the simulated GPP and  $\lambda$ ET improve at all levels and the improvements of  $\Delta$ RSME at all levels are  
 570 similar. However, as for  $\Delta$ RSME / MEAN shown in Figure 4 (c) and (i), the  $\lambda$ ET improvements are larger for  
 571 high VPD parts and GPP improvements are larger in the low VPD parts. This is due to that with low VPD,

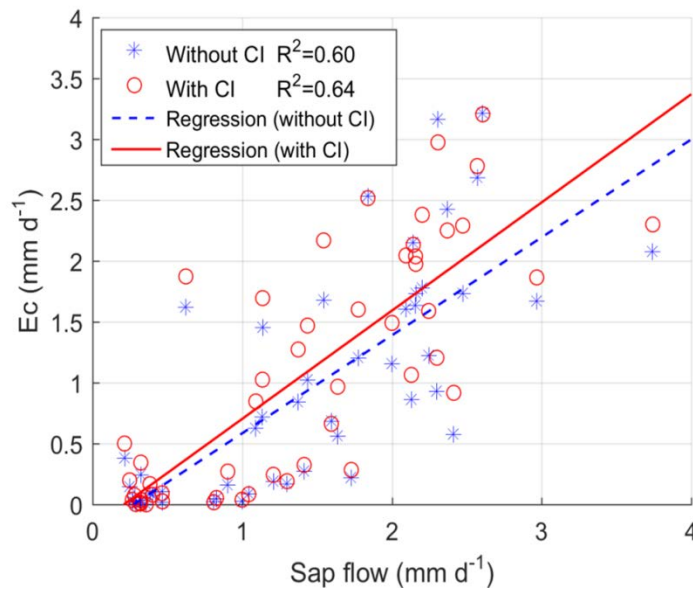
572 potential evapotranspiration was partitioned more into evaporation from intercepted water than transpiration,  
 573 according to Eq. (6) and (7). The model incorporates CI only into the transpiration module. This results in  
 574 limited improvement of  $\lambda ET$  in the low VPD part. However, the GPP improvements of  $\Delta RSME$  for all levels are  
 575 similar. The MEAN value of GPP is low. This leads to the high value of  $\Delta RSME / MEAN$  in Figure 4 (c). For  
 576 LAI, as shown in Figure 4 (d) and (j), improvements could be seen with different levels of LAI. For radiation  
 577 (Figure 4 (e) and (k)), the simulation improvements for GPP and  $\lambda ET$  are similar to VPD. This is due to that high  
 578 VPD and low radiation (low PAR and Rn-G) are concurrent. For different days of the year as shown in Figure 4  
 579 (f) and (l), the largest improvements occurred in the growing season from May to October. Generally, both GPP  
 580 and  $\lambda ET$  simulation improvements occur in the growing season, which coincides with higher temperatures and  
 581 larger incoming PAR.



582

583 Figure 4. The comparison of modeling performance without and with CI. The y-axis is the  $\Delta RMSE/MEAN$ . The  
 584 positive value indicates the simulation improvement, while the negative value means the simulation degradation.  
 585 (a~f) are for the GPP. (g~l) are for  $\lambda ET$ . (a) and (g) show the modeling improvement with various CI levels. (b)  
 586 and (h) are for  $T_a$ . (c) and (i) are for VPD. (d) and (j) correspond to various LAI levels. (e) and (k) are for  
 587 different PAR or  $R_n-G$  levels. (f) and (l) show the different day of year.

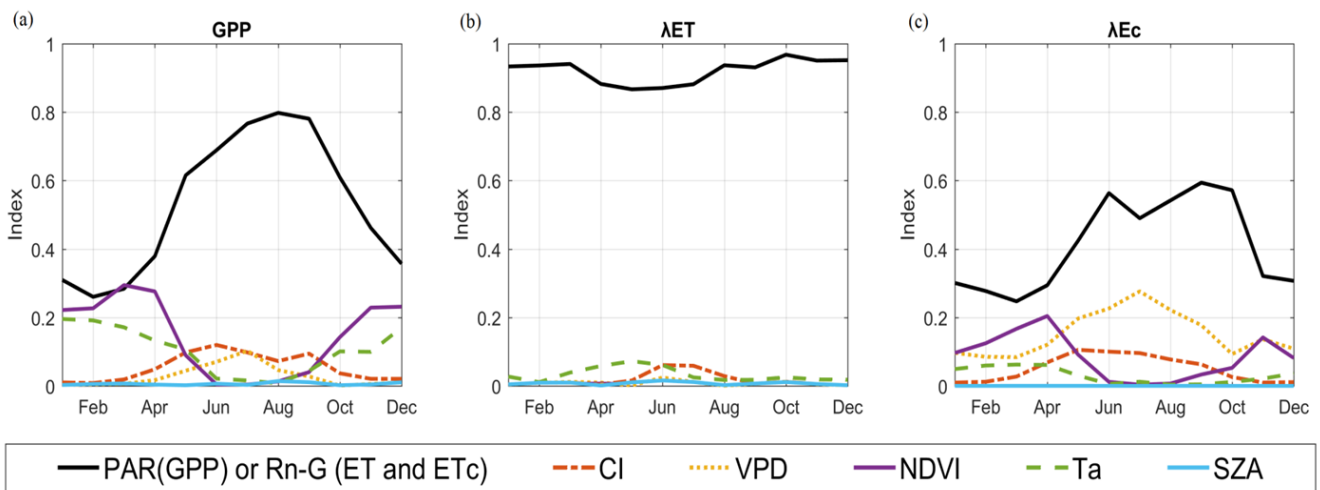
588 Comparison with sap flow measurements (Figure 5) shows that measurements fit slightly better with the  
 589 simulation with CI (red dots) than the simulation without CI (blue dots). The limited improvement is due to  
 590 model and observation uncertainties. For example, in the PT-JPL model, the relative surface wetness ( $f_{wet} =$   
 591  $RH^4$ ) was used to partition the evaporation from the intercepted rainfall and canopy transpiration. This empirical  
 592 formula might not be transferable without calibration to all sites and  $f_{wet}$  may not accurately partition  
 593 evaporation from the intercepted rainfall and canopy transpiration. Additionally, there are uncertainties related to  
 594 measurements of sap flow and upscaling sap flow data to the ecosystem level. However, the purpose is to  
 595 compare  $E_c$  and sapflow and to check whether there is an improvement of simulated  $E_c$ . With the current data  
 596 set, after incorporating CI into the model, the simulated transpiration improved as shown by the  $R^2$  increasing  
 597 from 0.60 to 0.64. This indicates that including CI could improve the simulation of transpiration. By comparing  
 598 the simulated  $\lambda ET$  of the same dates, the improvement for  $\lambda ET$  simulation with CI is small. After incorporating  
 599 CI, the RMSE of  $\lambda ET$  decreased from 13.99 to 13.73  $W \cdot m^{-2}$ . For  $R^2$ , the simulations with and without CI have  
 600 the same value of 0.92 (results not shown). This indicates incorporating CI may have limited improvement for  
 601 total ET, but the improvements on  $E_c$  are larger.



602  
 603 Figure 5. The scatterplot to evaluate transpiration ( $E_c$ ) with sap flow data (blue dots are simulation without CI  
 604 and red circles are simulation with CI)

605  
 606 4.3 Global sensitivity analysis (GSA)

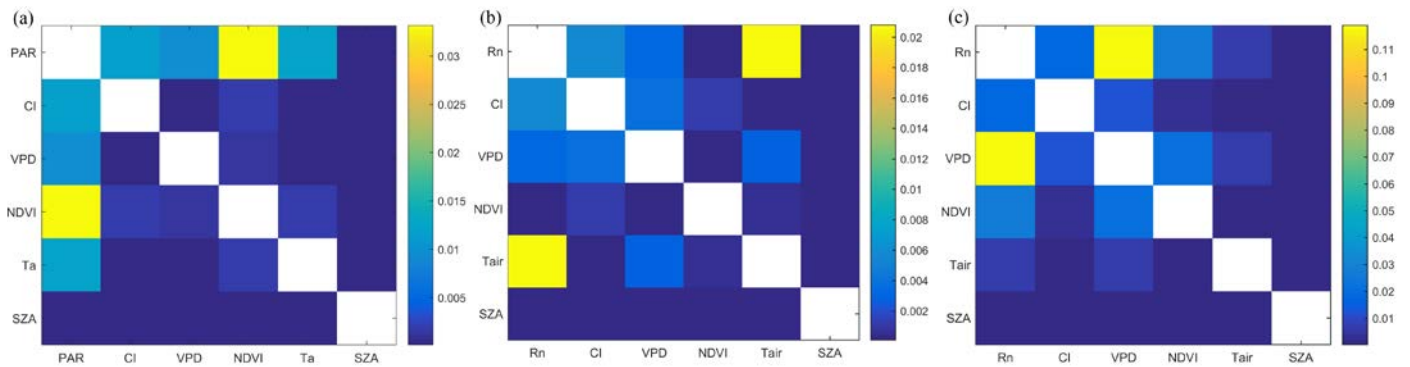
607 In this section, we aim to quantify the influence that CI has on GPP,  $\lambda ET$  and  $\lambda Ec$  and how it varies across  
 608 different months. The first order sensitivity represents the contribution of model forcing environmental variables  
 609 to GPP,  $\lambda ET$  and  $\lambda Ec$  (Figure 6). For GPP,  $\lambda ET$  and  $\lambda Ec$ , their variations are mainly regulated by the radiation  
 610 (PAR or Rn). This agrees with the direct effects from path analysis results, as shown in Table 4, indicating that  
 611 the ecosystem of this flux site is radiation controlled (van Dijk et al., 2005; Lagergren et al., 2008). Moreover,  
 612 similar to the direct effects from the path analysis, the effects of CI on GPP,  $\lambda ET$  and  $\lambda Ec$  are of similar  
 613 magnitude as those from VPD, air temperature and NDVI (which indicates LAI and phenology). Therefore, the  
 614 match between the direct effects revealed by path analysis and the first order sensitivity determined with GSA  
 615 confirms that the joint GPP and ET model can capture the major processes in this ecosystem. Furthermore, GSA  
 616 analysis also shows that sensitivities of GPP,  $\lambda ET$  and  $\lambda Ec$  vary substantially across different months (Fig.5). CI  
 617 had very limited contributions to the variability of GPP,  $\lambda ET$  and  $\lambda Ec$  in winter. The fact that there is a small  
 618 effect in winter, i.e. when the beech trees are without leaves, is due to the fact that there are ca. 20 % conifers in  
 619 the forest with a small contribution to the annual GPP. However, CI contributed more to the daily variability of  
 620 GPP,  $\lambda ET$  and  $\lambda Ec$  during the growing season, similar to the findings in our data driven analysis (Table 4) that  
 621 showed that  $\lambda ET^*$  and  $EF^*$  were more sensitive to the CI than  $\lambda ET$  and  $EF$  for the whole years. During the  
 622 growing season (from May to October), CI contributed to 11.88%, 3.04% and 7.78% of the total variability in  
 623 GPP,  $\lambda ET$  and  $\lambda Ec$ , respectively. The contribution from CI to GPP is the highest, followed by  $\lambda Ec$ . The  
 624 contribution to  $\lambda ET$  is less than that to  $\lambda Ec$  is due to soil evaporation is not sensitive to CI.



626 Figure 6. The first order Sobol' sensitivity index for the simulated GPP (a),  $\lambda ET$  (b) and  $\lambda Ec$  (c) for each month.  
 627 The variables are radiation components (PAR for GPP, Rn-G for  $\lambda ET$  and  $\lambda Ec$ ), CI, VPD, NDVI, Ta and SZA.

628 The second order sensitivity reveals interactions between the environmental variables and their joint effects on  
 629 the daily variability of GPP,  $\lambda ET$  and  $\lambda Ec$ . For GPP, as shown in Figure 7 (a), the clearest interaction is between  
 630 PAR and NDVI, indicating how changes in APAR determine GPP. For  $\lambda ET$ , as shown in Figure 7 (b), the  
 631 strongest interaction is again for energy and temperature variables: Rn and Ta. Second order sensitivities of  $\lambda Ec$   
 632 are shown in Figure 7 (c). Compared to GPP and  $\lambda ET$ , the second order sensitivities of  $\lambda Ec$  are higher indicating  
 633 more interactions among environmental variables to regulate the transpiration. The highest interaction for  $\lambda Ec$   
 634 is between Rn and VPD. CI mainly interacts with radiation (PAR or Rn-G) to control the GPP,  $\lambda ET$  and  $\lambda Ec$ ,

635 reflecting this ecosystem is radiation limited. This result also matches well with the path analysis in Table 5,  
 636 which CI has highest indirect effects on GPP,  $\lambda ET$  and  $\lambda ET^*$  through PAR or Rn-G. NDVI is the second most  
 637 important variable to interact with CI to jointly influence GPP. Similarly, in Table 5, LAI ranked as the second  
 638 important variable to deliver the indirect effects from CI to GPP. As for  $\lambda ET$  and  $\lambda Ec$ , VPD and NDVI are  
 639 important variables after Rn-G. Compared to Table 5, the indirect effects from CI through LAI and VPD to  $\lambda ET$   
 640 and  $\lambda ET^*$  are also significant. These results indicate that with potentially increasing levels of aerosols and  
 641 diffuse PAR over the growing season in the future, the WUE, LUE and EF will increase in principle, but the  
 642 magnitude of the enhancement will depend on the interplay between VPD and  $T_a$ .



643  
 644 Figure 7. The second order Sobol' sensitivity index for the simulated GPP (a),  $\lambda ET$  (b) and  $\lambda Ec$  (c) for the whole  
 645 year

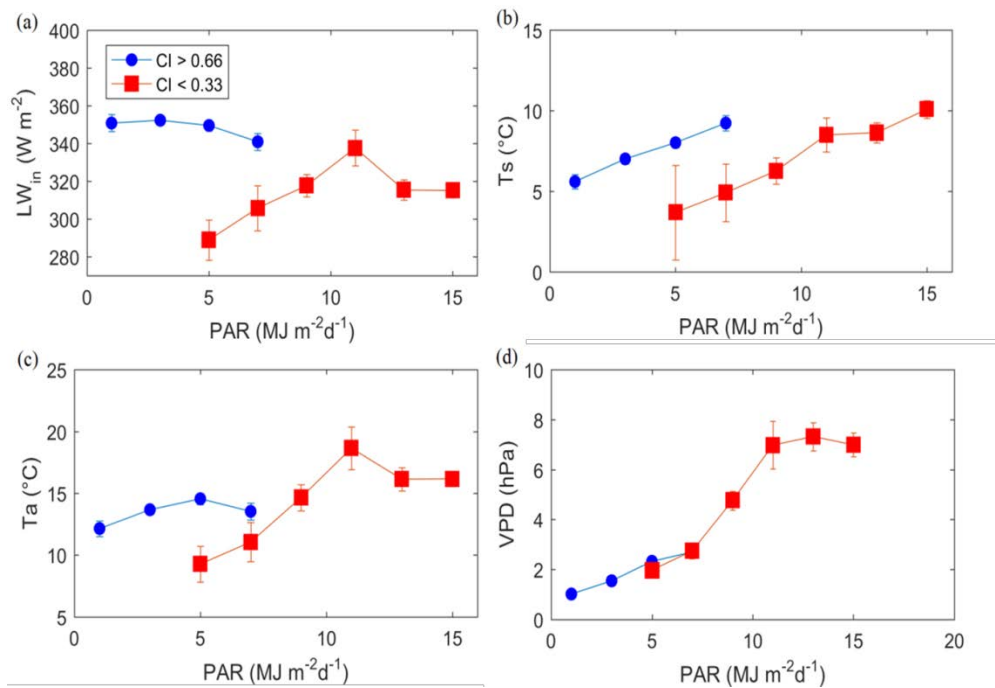
646

#### 647 4.4 Potential mechanism for diffuse PAR to influence GPP and ET of the Sorø beech forest site

648 Several mechanisms have been reported to explain the impacts of  $f_{diff}$  on GPP and ET. First, for the same levels  
 649 of PAR, diffuse PAR penetrates deeper into the canopies than direct PAR, and hence makes the vertical  
 650 distribution of PAR more even throughout forest canopies. Photosynthesis in the lower part of the canopy will be  
 651 stimulated by the increased diffuse PAR (Hollinger et al., 1994; Weiss, 2000; Oliphant et al., 2011). Second,  
 652 under clear-sky conditions, PAR is mainly direct, resulting in the photosynthesis of sunlit leaves being saturated,  
 653 whereas the photosynthesis rates of shaded leaves are constrained by the limited intercepted radiation. On cloudy  
 654 days, solar radiation is scattered by clouds in addition to atmospheric aerosols and the proportion of diffuse PAR  
 655 is high. The saturation effects of the sunlit leaves will be reduced (Gu et al., 2002). Furthermore, photosynthesis  
 656 and WUE may also benefit from reduced water and heat stress of plants when going from sunny and higher PAR  
 657 conditions to diffuse conditions (Gu et al., 2002; Lloyd et al., 2002; Steiner and Chameides, 2005; Urban et al.,  
 658 2012), especially for water limited ecosystems. Another possible reason for the high photosynthesis rate with  
 659 diffuse PAR is a change in spectral composition. Diffuse PAR has a higher ratio of blue to red bands than direct  
 660 PAR, which could stimulate photochemical reactions and stomatal opening (Urban et al., 2012; Cheng et al.,  
 661 2015).

662 It has been shown how in temperature-limited systems at high latitudes, incoming longwave radiation ( $LW_{in}$ )  
 663 under cloudy conditions is an important source of energy for snow melting by increasing the land surface

664 temperature (Juszak & Pelliciotti, 2013). We hypothesize that for a given total amount of PAR, increasing  
 665 diffuse fraction of PAR is associated with increased  $LW_{in}$  from clouds and aerosol, which should increase both  
 666 GPP and ET in temperature-limited conditions. To further explore this, the longwave radiative budget was  
 667 checked controlling for PAR (Figure 8 (a)). With more clouds,  $LW_{in}$  increased significantly ( $p<0.05$ ) for similar  
 668 incoming PAR. A clear effect of canopy warming (surface temperature,  $T_s$ ) via longwave radiative budget can  
 669 be seen in Figure 8 (b). In this temperature-limited ecosystem, increases in surface temperature (e.g. canopy  
 670 temperature) should enhance photosynthesis. For the air temperature ( $T_a$ ), we can also see the temperature  
 671 increase, but the increase of  $T_a$  is lower than that of  $T_s$ . Moreover, we also check the difference of VPD in  
 672 diffuse and direct radiation conditions, as shown in Figure 8 (d). It can be seen that VPD in diffuse and direct  
 673 radiation conditions was not significantly different within similar PAR levels. Even though in the long-term  
 674 dynamics (e.g. path analysis) lower VPD was linked to higher GPP and ET when controlling for PAR, changes  
 675 in VPD are not significant. Therefore, it can be seen that there is a possible mechanism in this ecosystem that  
 676 increase of long wave incoming due to more clouds could increase the surface temperature and further enhance  
 677 the photosynthesis rate. This leads to larger GPP and  $\lambda Ec$ .

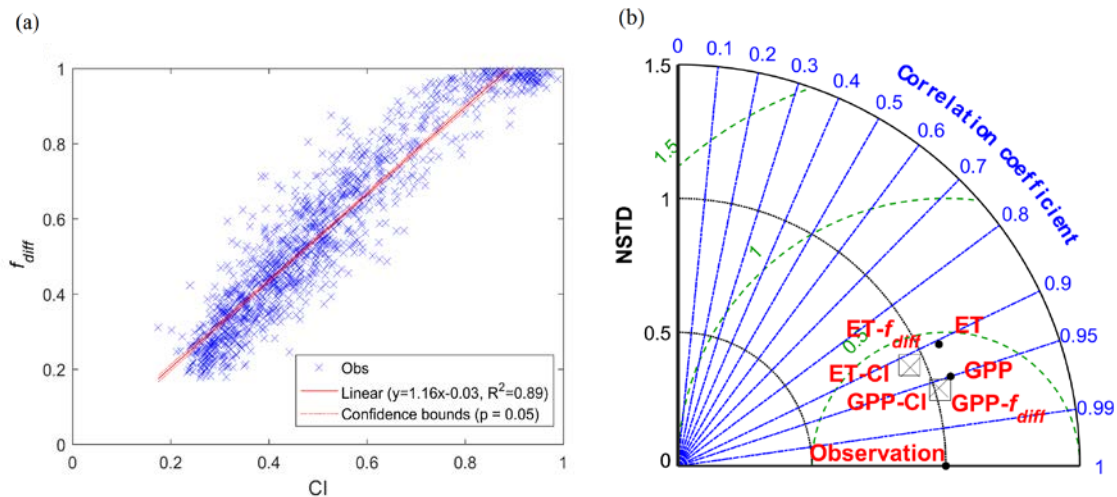


678  
 679 Figure 8. Responses of  $LW_{in}$  (a), canopy temperature  $T_s$  (b) and VPD (c) to various levels of PAR for  
 680 predominantly diffuse light condition (blue, CI>0.66) and predominantly direct light conditions (red, CI<0.33).  
 681 The points represent the mean value for specific incoming PAR interval and the error bar represent the  
 682 significance level at  $p<0.05$  ). To exclude the effects from phenology and obtain canopy temperature  $T_s$ ,  
 683 comparison was conducted with NDVI more than 0.75.

684

685 4.5 Comparison between CI and  $f_{diff}$

686 This study assumes that  $f_{diff}$  can be characterized by CI. The reason to use CI is its longer temporal availability  
 687 (2002-2012) at the Soroe flux site, while the observed  $f_{diff}$  was available only from 2004. Although previous  
 688 studies in the Netherlands and in tropical forest ecosystems have proven a strong relationship between  $f_{diff}$  and CI  
 689 (Spitters et al., 1986; Butt et al., 2010), this relationship might be different in high latitude areas. We performed  
 690 a statistical correlation test and model based analysis to check the difference between CI and  $f_{diff}$ . Figure 9 (a)  
 691 shows that CI and  $f_{diff}$  are highly correlated ( $R=0.94$ ). However, there is significant scatter when using the two  
 692 fractions at the daily time scale. This may be due to that in this study, we assume the PAR is equal to the half of  
 693 solar shortwave radiation and CI is actually calculated based on the whole range of solar radiation. However,  $f_{diff}$   
 694 is based on the observed diffuse and total PAR on the ground. The effects of scattering are wavelength  
 695 dependent, therefore CI and  $f_{diff}$  may behave differently. Additionally, in the atmosphere, there are two types of  
 696 wavelength dependent scattering: Rayleigh and Mie scattering. With different types of scattering, the  
 697 relationship between CI and  $f_{diff}$  may be influenced. However, even though the relationship between CI and  
 698  $f_{diff}$  shows some scatter, when we use these two indices as indicators of diffuse radiation in our modeling  
 699 framework, they show very similar simulation results, as shown in the Taylor Diagram of Figure 9 (b). The  
 700 simulation results are very similar. We therefore conclude that CI and  $f_{diff}$  are very similar and any of these  
 701 quantities could be used to represent the diffuse PAR in this region.



702  
 703 Figure 9. Comparison between  $f_{diff}$  and CI from 2004 to 2012. (a) the correlation test between CI and  $f_{diff}$  (b)  
 704 Taylor diagram comparing the GPP and ET modeling performance with CI (X) and  $f_{diff}$  (square) and without the  
 705 diffuse fraction (dot).

706

#### 707 4.6 Other factors that may potentially change responses of GPP and ET to diffuse PAR

708 This study evaluated the impact of diffuse PAR on GPP and ET, and assessed the interactions between CI and  
 709 other biophysical environmental variables to jointly regulate GPP and ET. Due to data availability and model  
 710 complexity, only environmental variables i.e. PAR, Rn-G, LAI, VPD, Ta and SWC were considered in the  
 711 analysis. Besides these biophysical variables, other variables providing an accurate estimate of the overall  
 712 fraction of absorbed PAR e.g. leaf inclination angle, leaf optical parameters (reflectance and transmittance) and

713 leaf-clumping index could influence the impacts of CI on GPP and ET. For instance, Knohl and Baldocchi (2008)  
714 found a 20% increase in diffuse PAR effects, when the leaf inclination angle increased from 40 to 70, using a  
715 canopy radiative transfer model. Variability in the orientation of leave surfaces also changes effects of diffuse  
716 PAR. Bonan (2002) suggested that the upper canopy leaves could utilize sunlight more efficiently when they  
717 have a near vertical orientation, while the lower foliage must almost be in a horizontal position. Knohl and  
718 Baldocchi (2008) highlighted that the clumped leave distribution could also have advantages for diffuse PAR.  
719 However, our study used top-down and parsimonious GPP and ET models and focused on the ecosystem scale.  
720 The impact of leaf properties throughout the whole canopy can thus not be analyzed in detail. The influence of  
721 diffuse PAR on evaporation of intercepted rainfall and soil water was also ignored. Diffuse PAR is more  
722 homogeneous than direct PAR. Diffuse PAR can penetrate deeper and radiation throughout the canopy and at the  
723 soil surface is more evenly distributed. This could contribute to not only higher transpiration rate but also more  
724 evaporation from soil and the intercepted water. According to Davin and Seneviratne (2012) the response of  
725 evaporation is less significant than the response of transpiration. This is also supported by our path analysis  
726 results. Therefore, in the PT-JPL model, CI was not incorporated in the parameterization of evaporation.

727

## 728 5. Conclusion

729 The effects of diffuse fraction of PAR on the carbon and water fluxes of a high latitude temperate deciduous  
730 forest ecosystem were evaluated using an 11-year (2002-2012) eddy covariance data set from a Danish flux site  
731 at Soroe. Using statistical analysis, this study identified that GPP, ET and WUE were mainly controlled by  
732 variables related with the radiation transfer in the canopy and net energy balance (PAR, LAI and Rn-G) while  
733 LUE and EF were primarily controlled by air temperature ( $T_a$ ). This indicates that this beech forest ecosystem is  
734 radiation and temperature limited. Diffuse PAR, expressed by the Cloudiness Index (CI), had positive direct  
735 effects on GPP, LUE, ET, EF and WUE. In terms of indirect effects, CI mainly interacted with the radiation  
736 components in the canopy (PAR, Rn-G and LAI) to influence GPP and ET.  $T_a$  and VPD were the major  
737 intermediate variables to deliver the indirect influence from CI to LUE and EF. These results indicate that with  
738 potentially increasing levels of aerosols and diffuse PAR over the growing season in the future, the WUE, LUE  
739 and EF will increase in principle, but the magnitude of the enhancement will depend on the interplay between  
740 VPD and  $T_a$ .

741 We tested a joint ‘top-down’ GPP and ET model, which combines a light use efficiency GPP model (Monteith et  
742 al, 1972) and Priestley–Taylor Jet Propulsion Laboratory ET model (Fisher et al., 2008). When incorporating CI  
743 into the simulations, the model performance for both GPP and ET improved with the RMSE of the daily GPP  
744 decreasing from 1.64 to 1.45  $\text{g}\cdot\text{C}\cdot\text{m}^{-2}\cdot\text{d}^{-1}$  (11.68% reduction) and the RMSE of the daily ET decreasing from  
745 15.79 to 14.50  $\text{W}\cdot\text{m}^{-2}$  (8.16% reduction). Based on a global sensitivity analysis (GSA), 11.88%, 3.04% and 7.78%  
746 of the variability of GPP, ET and transpiration, respectively, can be attributed to CI in the growing season from  
747 May to October. This proves that CI has largest impacts on GPP, followed by transpiration and finally ET, which  
748 results in higher WUE under diffuse fraction conditions. Even though the impact on ET is moderate, it was  
749 consistent and we found that most of the ET model improvements when incorporating CI could be linked to the  
750 transpiration component by comparing with sap flow measurements.

751 To explain the mechanisms behind GPP and evapotranspiration enhancement with diffuse radiation for fixed  
752 levels of PAR, most previous studies have focused on variables affecting the fraction of absorbed PAR. We  
753 found that the longwave emission from clouds and aerosols plays an additional role in this high latitude  
754 ecosystem. Under diffuse conditions and for same incoming PAR levels, higher longwave emission contributes  
755 to higher air and canopy temperature increasing both GPP and transpiration. This highlights the importance of  
756 improving the description of the complete radiative transfer in canopies under diffuse and direct conditions in  
757 high latitude deciduous forests to model GPP and ET.

758

### 759 **Acknowledgement:**

760 The authors would like to thank the EU and (Centre for the development of Industrial Technology (CDTI),  
761 Innovation Fund Denmark (IFD) and Flanders Innovation & Entrepreneurship (VLAIO)) for funding, in the  
762 frame of the collaborative international consortium FORWARD financed under the ERA-NET Cofund  
763 WaterWorks2015 Call. This ERA-NET is an integral part of the 2016 Joint Activities developed by the Water  
764 Challenges for a Changing World Joint Programme Initiative (Water JPI). We thank the editor and anonymous  
765 reviewers for their insightful comments and suggestions.

766

### 767 **References:**

- 768 Baldocchi, D.D., 2003. Assessing the eddy covariance technique for evaluating carbon dioxide exchange rates of  
769 ecosystems: past, present and future. *Glob. Change Biol.*, 9(4), 479-492.
- 770 Bassow, S.L., Bazzaz, F.A., 1998. How environmental conditions affect canopy leaf-level photosynthesis in four  
771 deciduous tree species. *Ecology*, 79(8), 2660-2675.
- 772 Boegh, E., Poulsen, R.N., Butts, M., et al., 2009. Remote sensing based evapotranspiration and runoff modeling  
773 of agricultural, forest and urban flux sites in Denmark: From field to macro-scale. *J. Hydrol.*, 377(3), 300-316.
- 774 Butt, N., New, M., Malhi, Y., et al., 2010. Diffuse radiation and cloud fraction relationships in two contrasting  
775 Amazonian rainforest sites. *Agr. Forest. Meteorol.*, 150(3), 361-368.
- 776 Chen, J., Jönsson, P., Tamura, M., et al., 2004. A simple method for reconstructing a high-quality NDVI time-  
777 series data set based on the Savitzky-Golay filter. *Remote Sens. Environ.*, 91(3), 332-344.
- 778 Chen, Y., Xia, J., Liang, S., et al., 2014. Comparison of satellite-based evapotranspiration models over terrestrial  
779 ecosystems in China. *Remote Sens. Environ.*, 140, 279-293.
- 780 Cheng, S. J., Bohrer, G., Steiner, A. L., et al., 2015. Variations in the influence of diffuse light on gross primary  
781 productivity in temperate ecosystems. *Agr. Forest. Meteorol.*, 201, 98-110.

782 Ciais, Ph, M. Reichstein, Nicolas Viovy, et al., 2005. Europe-wide reduction in primary productivity caused by  
783 the heat and drought in 2003. *Nature* 437, 7058: 529-533.

784 Davin, E. L., Seneviratne, S. I., 2012. Role of land surface processes and diffuse/direct radiation partitioning in  
785 simulating the European climate. *Biogeosciences*, 9(5), 1695–1707.

786 Donohue, R.J., Hume, I.H., Roderick, M.L., et al., 2014. Evaluation of the remote-sensing-based DIFFUSE  
787 model for estimating photosynthesis of vegetation. *Remote Sens. Environ.*, 155, 349-365.

788 Dunn, A. L., Barford, C. C., Wofsy, S. C., et al., 2007. A long-term record of carbon exchange in a boreal black  
789 spruce forest: Means, responses to interannual variability, and decadal trends, *Glob. Chang. Biol.*, 13, 577–590.

790 Ershadi, A., McCabe, M.F., Evans, J.P., et al., 2014. Multi-site evaluation of terrestrial evaporation models using  
791 FLUXNET data. *Agr. Forest. Meteorol.*, 187, 46-61.

792 Fisher, J.B., Tu, K.P. Baldocchi, D.D., 2008. Global estimates of the land–atmosphere water flux based on  
793 monthly AVHRR and ISLSCP-II data, validated at 16 FLUXNET sites. *Remote Sens. Environ.*, 112(3), 901-919.

794 García, M., Sandholt, I., Ceccato, P., et al., 2013. Actual evapotranspiration in drylands derived from in-situ and  
795 satellite data: Assessing biophysical constraints. *Remote Sens. Environ.*, 131, 103-118.

796 Gu, L.H., Baldocchi, D., Verma, S.B., et al., 2002. Advantages of diffuse radiation for terrestrial ecosystem  
797 productivity. *J. Geophys. Res.: Atmos.* 107, 4050.

798 Gu, L.H., Baldocchi, D.D., Wofsy, S.C., et al., 2003. Response of a deciduous forest to the Mount Pinatubo  
799 eruption: enhanced photosynthesis. *Science* 299, 2035–2038.

800 He, M., Ju, W., Zhou, Y., et al., 2013. Development of a two-leaf light use efficiency model for improving the  
801 calculation of terrestrial gross primary productivity. *Agr. Forest. Meteorol.*, 173, 28-39.

802 Heald, C. L., Henze, D. K., Horowitz, L. W., et al. 2008. Predicted change in global secondary organic aerosol  
803 concentrations in response to future climate, emissions, and land use change. *J. Geophys. Res.: Atmos.*, 113.D5.

804 Healy, K.D., Ricker, K.G., Hammer, G.L., Bange., M.P., 1998. Radiation use efficiency increases when the  
805 diffuse component of incident radiation is enhanced. *Aust. J. Agric. Res.* 49:665– 672.

806 Hollinger, D. Y., Kelliher, F. M., Byers, J. N., Hunt, J. E., McSeveny, T. M., Weir, P. L., 1994. Carbon dioxide  
807 exchange between an undisturbed old growth temperate forest and the atmosphere. *Ecology*, 75(1), 134-150.

808 Houborg, R., Anderson, M.C., Norman, J.M., Wilson, T., Meyers, T., 2009. Intercomparison of a ‘bottom-  
809 up’and ‘top-down’ modeling paradigm for estimating carbon and energy fluxes over a variety of vegetative  
810 regimes across the US. *Agr. Forest. Meteorol.*, 149(11), 1875-1895.

811 Houborg, R.M. Soegaard, H., 2004. Regional simulation of ecosystem CO<sub>2</sub> and water vapor exchange for  
812 agricultural land using NOAA AVHRR and Terra MODIS satellite data. Application to Zealand,  
813 Denmark. *Remote Sens. Environ.*, 93(1), 150-167.

- 814 Huxman, T.E., Turnipseed, A.A., Sparks, J.P., Harley, P.C., Monson, R.K., 2003. Temperature as a control over  
815 ecosystem CO<sub>2</sub> fluxes in a high-elevation, subalpine forest. *Oecologia*, 134(4), 537-546.
- 816 Ibrom, A., Jarvis, P.G., Clement, R., et al., 2006. A comparative analysis of simulated and observed  
817 photosynthetic CO<sub>2</sub> uptake in two coniferous forest canopies. *Tree Physiol.*, Victoria- 26, 7: 845.
- 818 Impens, I., Lemur, R., 1969. Extinction of net radiation in different crop canopies. *Theor. Appl. Climatol.*, 17,  
819 403–412.
- 820 Kanniah, K.D., Beringer, J., North, P. Hutley, L., 2012. Control of atmospheric particles on diffuse radiation and  
821 terrestrial plant productivity: A review. *Prog. Phys. Geog.*, 36(2), 209-237.
- 822 Knohl, A., Baldocchi, D. D., 2008. Effects of diffuse radiation on canopy gas exchange processes in a forest  
823 ecosystem. *J. Geophys. Res.: Biogeosci.* 113.G2 .
- 824 Lagergren, F., Lindroth, A., Dellwik, E., et al., 2008. Biophysical controls on CO<sub>2</sub> fluxes of three northern  
825 forests based on long-term eddy covariance data. *Tellus B*, 60(2), 143-152.
- 826 Lhomme, J.P., 1997. A theoretical basis for the Priestley-Taylor coefficient. *Bound-Lay. Meteorol.*, 82(2), 179-  
827 191.
- 828 Li, C.C., 1975. *Path analysis-a primer*. The Boxwood Press.
- 829 Lohammer T., Larsson S., Linder S. Falk S.O., 1980. FAST simulation models of gaseous exchange in Scots  
830 Pine. *Ecol. Bull.*, 32, 505-523.
- 831 McCallum, I., Wagner, W., Schmulius, C., Shvidenko, A., Obersteiner, M., Fritz, S. Nilsson, S., 2009. Satellite-  
832 based terrestrial production efficiency modeling. *Carbon balance and management*, 4(1), 8.
- 833 Mercado, L.M., Bellouin, N., Sitch, S., Boucher, O., Huntingford, C., Wild, M., Cox, P.M., 2009. Impact of  
834 changes in diffuse radiation on the global land carbon sink. *Nature* 458, 1014–1087.
- 835 Michel, D., Jiménez, C., Miralles, D. M., et al., E. F. Wood, and D. Fernández-Prieto, 2016. The WACMOS-ET  
836 project – Part 1: Tower-scale performance of four observation-based evapotranspiration algorithms, *Hydrol.*  
837 *Earth Syst. Sci.*, 20, 803-822.
- 838 Miralles, D. G, Jiménez, C., Jung, M., et al., 2016. The WACMOS-ET project - Part 2: Evaluation of global land  
839 evaporation data sets, *Hydrol. Earth Syst. Sci.*, 20, 823-842.
- 840 Mo, X., Liu, S., 2001. Simulating evapotranspiration and photosynthesis of winter wheat over the growing  
841 season, *Agr. Forest. Meteorol.*, 109, 203–222.
- 842 Monteith, J.L., 1972. Solar radiation and productivity in tropical ecosystems. *J. Appl. Ecol.*, 9(3), 747-766.
- 843 Mu, Q., Heinsch, F.A., Zhao, M., Running, S.W., 2007. Development of a global evapotranspiration algorithm  
844 based on MODIS and global meteorology data. *Remote Sens. Environ.*, 111(4), 519-536.

- 845 Oliphant, A. J., Dragoni, D., Deng, B., et al., 2011. The role of sky conditions on gross primary production in a  
846 mixed deciduous forest. *Agr. Forest. Meteorol.*, 151(7), 781-791.
- 847 Oliveira, P.J., Davin, E.L., Levis, S., Seneviratne, S.I., 2011. Vegetation-mediated impacts of trends in global  
848 radiation on land hydrology: a global sensitivity study. *Glob. Change Biol.*, 17(11), 3453-3467.
- 849 Orgill, J.F., Hollands, K.G.T., 1977. Correlation equation for hourly diffuse radiation on a horizontal surface. *Sol.*  
850 *Energy*, 19(4), 357-359.
- 851 Pilegaard, K., Hummelshøj, P., Jensen, N.O., Chen, Z., 2001. Two years of continuous CO<sub>2</sub> eddy-flux  
852 measurements over a Danish beech forest. *Agr. Forest. Meteorol.*, 107(1), 29-41.
- 853 Pilegaard, K., Ibrom, A., Courtney, M.S., Hummelshøj, P., Jensen, N.O., 2011. Increasing net CO<sub>2</sub> uptake by a  
854 Danish beech forest during the period from 1996 to 2009. *Agr. Forest. Meteorol.*, 151(7), 934-946.
- 855 Potter, C.S., Randerson, J.T., Field, C.B., et al., 1993. Terrestrial ecosystem production: a process model based  
856 on global satellite and surface data. *Global Biogeochem. Cycles*, 7(4), 811-841.
- 857 Rocha, A.V., Su, H.B., Vogel, C.S., Schmid, H.P. Curtis, P.S., 2004. Photosynthetic and water use efficiency  
858 responses to diffuse radiation by an aspen-dominated northern hardwood forest. *Forest Sci.*, 50(6), 793-801.
- 859 Roderick, M.L., Farquhar, G.D., Berry, S.L. and Noble, I.R., 2001. On the direct effect of clouds and  
860 atmospheric particles on the productivity and structure of vegetation. *Oecologia*, 129(1), 21-30.
- 861 Ross, J., 1976. Radiative transfer in plant communities. In J. L. Monteith (Ed.), *Vegetation and the atmosphere*  
862 (13-56). London: Academic Press.
- 863 Running, S.W., Nemani, R.R., Heinsch, F.A., Zhao, M., Reeves, M., Hashimoto, H., 2004. A continuous  
864 satellite-derived measure of global terrestrial primary production. *Bioscience*, 54(6), 547-560.
- 865 Ruimy, A., Kergoat, L., Bondeau, A., Intercomparison, T., Model, P.O.T.P.N., 1999. Comparing global models  
866 of terrestrial net primary productivity (NPP): Analysis of differences in light absorption and light use efficiency.  
867 *Glob. Change Biol.*, 5(S1), 56-64.
- 868 Ryu, Y., Baldocchi, D.D., Kobayashi, H., et al., 2011. Integration of MODIS land and atmosphere products with  
869 a coupled process model to estimate gross primary productivity and evapotranspiration from 1 km to global  
870 scales. *Global Biogeochem. Cycles*, 25(4).
- 871 Saltelli, A., Annoni, P., Azzini, I., Campolongo, F., Ratto, M., Tarantola, S., 2010. Variance based sensitivity  
872 analysis of model output. Design and estimator for the total sensitivity index. *Comput. Phys. Commun.*, 181,  
873 259–270.
- 874 Schiermeier, Q., 2006. Oceans cool off in hottest years. *Nature* 442, 854–855.
- 875 Sobol, I.M., 2001. Global sensitivity indices for nonlinear mathematical models and their Monte Carlo estimates.  
876 *Math Comput. Simulat.*, 55(1), 271-280.

877 Spitters, C.J.T., 1986. Separating the diffuse and direct component of global radiation and its implications for  
878 modeling canopy photosynthesis Part II. Calculation of canopy photosynthesis. *Agr. Forest. Meteorol.*, 38(1-3),  
879 231-242.

880 Steiner, A.L., Chameides, W.L., 2005. Aerosol-induced thermal effects increase modeled terrestrial  
881 photosynthesis and transpiration. *Tellus B* 57 (5), 404–411.

882 Stroosnijder, L., Moore, D., Alharbi, A., Argaman, E., Biazin, B., van den Elsen, E., 2012. Improving water use  
883 efficiency in drylands. *Curr. Opin. Environ. Sustain.*, 4(5), 497-506.

884 Taylor, K.E., 2001. Summarizing multiple aspects of model performance in a single diagram. *J. Geophys. Res.:*  
885 *Atmos.*, 106(D7), 7183-7192.

886 Turner, D.P., Urbanski, S., Bremer, D., et al., 2003. A cross-biome comparison of daily light use efficiency for  
887 gross primary production. *Glob. Change Biol.*, 9(3), 383-395.

888 Urban, O., Klem, K., Ač, A., Havránková, K., et al., 2012. Impact of clear and cloudy sky conditions on the  
889 vertical distribution of photosynthetic CO<sub>2</sub> uptake within a spruce canopy. *Funct. Ecol.* 26 (1), 46–55.

890 Van de Griend, A.A., Owe, M., 1993. On the relationship between thermal emissivity and the normalized  
891 difference vegetation index for natural surfaces. *Int. J. Remote Sens.*, 14(6), 1119-1131.

892 van Dijk, A.I., Dolman, A.J. Schulze, E.D., 2005. Radiation, temperature, and leaf area explain ecosystem  
893 carbon fluxes in boreal and temperate European forests. *Global Biogeochem. Cy.*, 19(2).

894 Vinukollu, R.K., Meynadier, R., Sheffield, J., Wood, E.F., 2011. Multi-model, multi-sensor estimates of global  
895 evapotranspiration: climatology, uncertainties and trends. *Hydrol. Process.*, 25(26), 3993-4010.

896 Vinukollu, R.K., Wood, E.F., Ferguson, C.R., Fisher, J.B., 2011. Global estimates of evapotranspiration for  
897 climate studies using multi-sensor remote sensing data: Evaluation of three process-based approaches. *Remote*  
898 *Sens. Environ.*, 115(3), 801-823.

899 Wang, S., Huang, K., Yan, H., et al., 2015. Improving the light use efficiency model for simulating terrestrial  
900 vegetation gross primary production by the inclusion of diffuse radiation across ecosystems in China. *Ecol.*  
901 *Complex.*, 23, 1-13.

902 Wang, Y.P., Leuning, R., 1998. A two-leaf model for canopy conductance, photosynthesis and partitioning of  
903 available energy I: Model description and comparison with a multi-layered model. *Agr. Forest. Meteorol.*, 91(1),  
904 89-111.

905 Weiss, S.B. 2000. Vertical and temporal distribution of insolation in gaps in an old-growth coniferous forest.  
906 *Can. J. For. Res.* 30:1953–1964.

907 Williams, I.N., Riley, W.J., Kueppers, L.M., Biraud, S.C., Torn, M.S., 2016. Separating the effects of phenology  
908 and diffuse radiation on gross primary productivity in winter wheat. *J. Geophys. Res.: Biogeosci.*, 121(7), 1903-  
909 1915.

- 910 Wu, J., Albert, L. P., Lopes, A. P., et al., 2016. Leaf development and demography explain photosynthetic  
911 seasonality in Amazon evergreen forests. *Science*, 351(6276), 972–976.
- 912 Wu, J., Linden, L. V. D., Lasslop, G., et al., 2012. Effects of climate variability and functional changes on the  
913 interannual variation of the carbon balance in a temperate deciduous forest. *Biogeosciences*, 9(1), 13-28.
- 914 Yuan, W., Cai, W., Xia, J., et al., 2014. Global comparison of light use efficiency models for simulating  
915 terrestrial vegetation gross primary production based on the LaThuile database. *Agr. Forest. Meteorol.*, 192, 108-  
916 120.
- 917 Zhou, Y., Wu, X., Ju, W., et al., 2015. Global parameterization and validation of a two-leaf light use efficiency  
918 model for predicting gross primary production across FLUXNET sites. *J. Geophys. Res.: Biogeosci.* 121.4:  
919 1045-1072.